MINISTRY OF THE HIGH AND SPECIALIZED SECONDARY EDUCATION OF REPUBLIC OF UZBEKISTAN

National University of Uzbekistan named Mirzo Ulugbek

Bozorova Dil'bar

Magnetooptical and optical properties of the rare-earth paramagnetic glasses

BACHELOR THESIS
In Optical Physics

This work was reviewed and is allowed to the protection.
The head of the department of Optics and Laser Physics,
PhD, Associate Professor
T. Akhmadjanov _____
"____"_____ 2013 г.

Scientific adviser,
Doctor of Phys. Sciences,
Professor
U.V. Valiev _____

Tashkent – 2013

CONTENS

INTRODUCTION

Present-day magnetooptics is a part of modern physics arising at the junction of two branches of knowledge - physical optics and physics of magnetic phenomena and covering a wide range of problems regarding the anisotropy associated with optical features of materials placed in an external magnetic field H. In fact, the disturbance of the medium by the magnetic field manifests itself as a difference in the optical characteristics of the medium (absorption, refraction, *etc*.) for clockwise and counter-clockwise circularly polarized light radiation, and as the circular anisotropy of secondary radiation spectra (luminescence, combinational scattering, *etc*.). These effects, which differ greatly with respect to both the experimental methods used and the nature of the information extracted from the data, have continued to attract the attention of numerous investigators over many years.

In the early stages of the intensive development of magnetooptical studies that began in the 1960's and 1970's, the focus of researches was directed toward producing new magnetic rare-earth (RE) dielectrics characterized by large magnetooptical effects and high transparency within the visible and near infrared (IR) frequency range of the material. The astonishing results of these initial investigations quickly led to opportunities for the development of technical applications of these magnetooptical effects in the now well-recognized fields of photonics, optoelectronics, and microelectronics. In addition, there is considerable interest in the fundamental investigation of the magnetooptics of rare-earth magnetic dielectrics, as they provide an opportunity to solve fundamental problems in the physics of magnetic phenomena in solids. Namely, they provide the opportunity to gain deeper understanding and interpretation of the inter-relationship between the magnetooptical effects and magnetization, on the one hand, and the features of the energy spectrum formed by the crystalline electric environment of a RE-ion in these magneto-dielectrics, on the other hand. Due to the high sensitivity of the magnetooptical effects (differential in essence) to external physical influences, these studies have allowed the investigator to obtain

important and unique information not obtainable by other physical methods traditionally used to study the electronic structure, energy spectra, and wavefunctions of RE-compounds. Obvious advantages to this approach, as described in this text, are the relatively simple modeling and calculation techniques that are available to interpret the magnetooptical spectra. Due to the highly selective nature and spin sensitivity of the magnetooptical effects, detailed results become available that cannot be observed in the analyses of optical spectra obtained from data produced by more traditional methods, including polarized absorption and fluorescence spectra.

Nowadays, Er^{3+} doped optical materials have attracted great interest due to their possible application as media for the up-conversion laser, waveguide laser and Er^{3+}-doped fiber amplifier (EDFA), which is one of key elements used in the wavelength division multiplexing (WDM) network system for optical communication. Since oxyfluoride glass ceramics were applied effectively relatively recently, oxyfluoride glass ceramics doped with RE-ions have been researched widely in the past few decades, because they possess not only higher chemical and mechanical stability than fluoride glass but also lower phonon energy than oxide glass. Due to the fact that the thermal treatment close to the crystallization temperature for the oxyfluoride glasses, transparent oxyfluoride glass ceramics can be obtained, in which fluoride crystallites are dispersed in the oxide glass matrix. If the RE-ions can be successfully incorporated into the fluoride crystals which can provide a low phonon environment, rare-earth ion doped glass ceramics will exhibit excellent luminescence properties.

In connection with that, we have examined below some interesting aspects of the transparent oxyfluoride glass ceramics doped by Er^{3+}/Yb^{3+} ions the magnetooptical and optical properties due to the high optical resolution and sensitivity of the magnetooptical methods providing the reliable detecting of the changes in the energies and linewidths of the optical transitions are caused by an external magnetic field and taking place in the RE-compounds.

Chapter 1. OPTICAL AND MAGNETOOPTICAL PROPERTIES OF THE RARE-EARTH PARAMAGNETIC GLASSES

§1.1. Electronic structure of the rare-earth ions

In rare-earth (RE) compounds, the lanthanide ions (from Ce^{3+} to Yb^{3+}) are usually found in the trivalent state RE^{3+}. The ground electronic configuration of the RE -ions may be written as [Xe]$4f^n$, where [Xe] = $1s^2 2s^2 2p^6 3s^2 3p^6 3d^{10} 4s^2 4p^6 4d^{10} 5s^2 5p^6$ is the closed-shell configuration of the noble gas xenon, and n is the number of electrons in the unfilled $4f^n$ shell ranging from $n = 1$ for Ce^{3+} to $n = 13$ for Yb^{3+}. The characteristic magnetic moment for each RE-ion leads to an interaction between that ion and an applied external magnetic field H, producing interesting magnetic and magnetooptical features in the RE compounds.

Over the years, methods of numerical analysis have been developed to calculate the energy states of "free" RE-ions (that is, for ions that are not in a ligand or crystal-field environment). These methods allow evaluation of the multiplicities of states and the energy-level positions of excited electronic configurations relative to the ground state. Energy intervals for $4f^n$, $4f^{n-1}5d$, $4f^{n-1}6s$, and other excited electronic configurations for free RE-ions are presented in Refs. [1-2]. Also presented are energy level schemes for the energy levels of the $4f^n$ configuration for all trivalent RE-ions. From these results it follows that the excited RE-ion configurations, such as $4f^{n-1}5d$, $4f^{n-1}6s$, are separated from the $4f^n$ ground state by an energy interval typically on the order of 10^5 cm^{-1}.

The repulsion between the equivalent $4f$ electrons within the shell, usually called the correlation Coulomb interaction of the RE-ion, splits the states into *terms* characterized by the orbital (L) and spin (S) momenta. A *term* with fixed values of L and S has $(2L + 1)(2S + 1)$ degenerate states distinguished by the m_L and m_S projections of the orbital and spin momenta. The wave functions of these degenerate states are given by $|\gamma LSm_L m_S\rangle$, where $-L \le m_L \le L$, $-S \le m_S \le S$ and the

index γ distinguishes between terms with the same L and S. Neighboring terms are separated from each other by an energy interval on the order of ~10^4 cm^{-1} [3-5].

To determine the ground term of the $4f^n$ electronic configuration, one usually applies Hund's rules and the Pauli exclusion principle [4,6]. Hund's first two rules assert:

1) For a given electronic configuration the *term* (i.e., a quantum state with fixed $\boldsymbol{L}$ and $\boldsymbol{S}$) with maximum multiplicity (i.e., with maximum $\boldsymbol{S}$) has the lowest energy.
2) For a given multiplicity (i.e., $\boldsymbol{S} = \boldsymbol{S}_{max}$), the *term* with the largest value of $\boldsymbol{L}$ has the lowest energy.

For instance, let us apply Hund's rules for the determination of the ground term of the rare-earth Tb^{3+} ion that has eight electrons in the unfilled $4f^8$ electronic configuration. In this regard, we can construct Table 1.1 for the orbital (m_l) and spin (m_s) momentum projections of the eight *f* electrons. Hund's first rule indicates that the first seven electrons will fill states of the same spin momentum (m_s); Hund's second rule indicates that the eighth electron will fill one of the remaining (opposite-spin) states having the largest angular momentum (m_l). This is shown in **Table 1.** In spectroscopic language, the ion Tb^{3+} has a ground term of ^7F, where the conventional notation is $^{(2S+1)}L$ with $(2S+1)$ being the *multiplicity*.

Table 1. *Arrangement of the orbital (m_l) and spin (m_s) momentum projections in the $4f^8$ electronic configuration of Tb^{3+}. The maximum number of f electrons in the shell is N = 14.*

m_s \ m_l	-3	-2	-1	0	+1	+2	+3
↑	↑	↑	↑	↑	↑	↑	↑
↓	↓						↓

The quantum degeneracy of the RE-ion terms is removed by the spin-orbit interaction W_{SO} that has a value on the order of ~10^3 cm^{-1}. The effective Hamiltonian of the spin-orbit interaction that describes the splitting of the term with fixed values of L and S has the form,

$$\hat{H}_{LS} = \xi \cdot \hat{L} \cdot \hat{S}, \qquad (1.1)$$

where $\hat{L}$ and $\hat{S}$ are the operators of the orbital and spin momenta, respectively, and ξ is the spin-orbit coupling constant defined by the well-known Goudsmit formula [5]. From a qualitative point of view, the spin-orbit interaction W_{SO} corresponds to the magnetic interaction between the spin magnetic momentum and the magnetic field caused by the motion of the 4*f* electron around the nucleus. In the one-electron approximation, W_{SO} can be written as [7],

$$W_{SO} = \frac{\hbar^2 e^2 (\vec{l} \cdot \vec{s})}{2m^2 c^2 \cdot r^3}, \qquad (1.2)$$

where $\hbar$ is the Plank constant, m and e are the mass and charge of the electron, c is the speed of light, r is the radius of electron orbit, and ***l*** and ***s*** are the orbital and spin moments of the electron, respectively.

The spin-orbit interaction splits the $^{(2S+1)}L$-terms into multiplets characterized by the total angular momentum J (with $|L - S| \le J \le L + S$) whose wavefunctions are spherical functions expressed in terms of $|J,M_J\rangle$ [8]. Each multiplet is many-fold degenerate in terms of its angular momentum projection M_J; this degeneracy can be removed by an external action (relative to the RE-ion), such as crystalline electric or magnetic fields. In the case of an applied external magnetic field, H, a complete lifting of the degeneracy takes place, with the $^{(2S+1)}L_J$ multiplet split into $(2J + 1)$ equidistant sublevels. The energy interval between sublevels is defined by the magnetic field intensity and by the value of the g-factor. We write the Hamiltonian (1.1) in the form,

$$\hat{H}_{LS} = \frac{1}{2}\xi \cdot \left(\hat{J}^2 - \hat{L}^2 - \hat{S}^2\right). \qquad (1.3)$$

For the diagonal matrix elements that define the multiplet energy E we obtain,

$$E(J) = \frac{1}{2}\xi \cdot \left[J(J+1) - L(L+1) - S(S+1)\right]. \qquad (1.4)$$

From this expression, the Lande' "rule of intervals" is determined as,

$$E(J) - E(J-1) = \frac{1}{2}\xi \cdot \left[J(J+1) - J(J-1)\right] = \xi \cdot J\,, \qquad (1.5)$$

which gives the difference in energy between neighboring multiplets having the same L and S [3].

The nomenclature of the multiplets in a term depends on the sign of the spin-orbit coupling constant ξ. For the "heavy" RE-ions (from Tb^{3+} to Yb^{3+}) with the 4*f* shell more than half filled $\xi < 0$, so the lowest-energy multiplet will have the largest possible value of J for a given L and S, that is, $J_0 = L_0 + S_0$. For the "light" RE-ions (from Ce^{3+} to Gd^{3+}) with less than a half-filled 4*f* shell, $\xi > 0$. In this case, the lowest-energy multiplet will have the smallest possible value of J for a given L and S, that is, $J_0 = |L_0 - S_0|$. This is known as Hund's third rule, which asserts that:

3) For the less-than-half filled shell, the state with the smallest allowed value of J is the lowest energy state; for the more-than-half filled shell, the state with the largest allowed value of J is the lowest energy state.

A general scheme for the energy spectrum for the $4f^n$ configuration of the free rare earth ion based on these energy terms is presented in Fig. 1. The ground term for each trivalent RE-ion and the ground and first excited multiplets associated with each of these terms in the $4f^n$ configuration are presented in **Table 2.**

The classification of free-RE ion states is based on the Russell-Saunders approximation (also called normal- or *LS*-coupling), which requires that the energy separation between the terms be much greater than the value of the term-splitting into multiplets by the spin-orbit interaction. For the ground term of the $4f^n$ configuration, this approximation is generally valid. However, significant deviation from *LS*-coupling is observed for excited RE-ion states [3,4]. Nevertheless, *LS*-coupling is still a sufficiently good approximation to calculate the energy spectra and the classification of states for both the ground $4f^n$ configuration and the lower states of the first excited $4f^{n-1}5d$ and $4f^{n-1}6s$ configurations of the free RE-ions. As shown by the results from direct calculations (see, for example, Refs. [9,10]), the energy value of the *d* electron interaction with the *f* electrons of the $4f^{n-1}$ "core" of

the $4f^{n-1}5d$ configuration is on the order of ~10^4 cm^{-1}, while the value of the spin-orbit interaction for the *d* electron is on the order of ~10^3 cm^{-1}. The lower states of the $4f^{n-1}5d$ (or $4f^{n-1}6s$) configuration of the free RE ion can be described in the *LS*-coupling approximation as vector sums of the quantum numbers *L* and *S* that characterize the ground state of the $4f^{n-1}$ "core" with the quantum numbers *l* and *s* of the "valence" 5*d* (or 6*s*) electron [4,5,7].

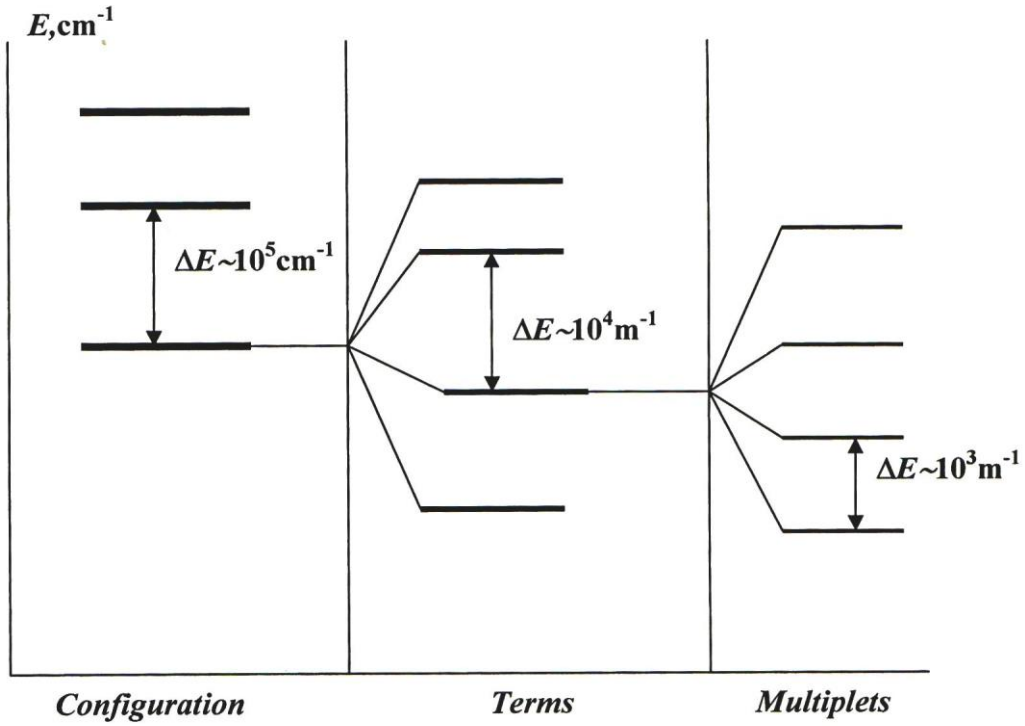

Fig. 1. Splitting scheme for the energy levels of the free rare-earth ions [3].

Table 2. Ground and first excited energy levels of the free RE-ions.

RE^{3+}	Ground electronic configuration	Ground term	Ground multiplet	First excited multiplet	$E_1 - E_0$ (cm^{-1})
Ce	$4f^1$	^2F	$^2F_{5/2}$	$^2F_{7/2}$	2200
Pr	$4f^2$	^3H	$^3H_4$	$^3H_5$	2200
Nd	$4f^3$	^4I	$^4I_{9/2}$	$^4I_{11/2}$	1800
Pm	$4f^4$	^5I	$^5I_4$	$^5I_5$	1600
Sm	$4f^5$	^6H	$^6H_{5/2}$	$^6H_{7/2}$	1000
Eu	$4f^6$	^7F	$^7F_0$	$^7F_1$	350
Gd	$4f^7$	^8S	$^8S_{7/2}$	–	–
Tb	$4f^8$	^7F	$^7F_6$	$^7F_5$	2300
Dy	$4f^9$	^6H	$^6H_{15/2}$	$^6H_{13/2}$	3400
Ho	$4f^{10}$	^5I	$^5I_8$	$^5I_7$	5000
Er	$4f^{11}$	^4I	$^4I_{15/2}$	$^4I_{13/2}$	6400
Tm	$4f^{12}$	^3H	$^3H_6$	$^3H_5$	8200
Yb	$4f^{13}$	^2F	$^2F_{7/2}$	$^2F_{5/2}$	10100

It is well-known that the crystalline environment plays an important role in the formation of the electronic properties of the rare earth (RE) ions in crystals [3]. Due to the "shielding" of the 4*f* valence electrons from the environment by the filled 5*s* and 5*p* shells (see §1.1), the crystal field (CF) interaction is substantially smaller than the spin-orbit coupling ($W_{CF} << W_{SO}$). This allows the CF to be considered as a weak perturbation acting on a free atomic or ionic energy level, with the multiplet structure (due to the interaction between the orbital and spin momenta of the 4*f* electron system) remaining nearly constant. However, the behavior of the RE-ions will be quite different in the presence of the crystal field, depending on whether there is an even or an odd number of electrons in the unfilled ($4f^n$) electronic shell. The differences in the observed spectra are explained by the Kramers theorem [3]. That is, for ions with an odd number of electrons in the 4*f* electronic shell, resulting in a half-integral total spin, the orbital degeneracy is removed completely by the low-symmetry CF because the crystal field directly

influences the orbital motion of the electron. The spin degeneracy is reduced by the "pairing" of electrons with oppositely oriented spins, i.e., the RE -ion goes from a high-spin state to a low-spin state. However, there remains one extra "unpaired" electron with spin in a degenerate state. Such degeneracy cannot be removed by either crystalline or orbital interaction, but can be removed by an external magnetic field (or an exchange field). By contrast, the spin degeneracy can be removed completely for ions with an even number of electrons, as all of the electrons may be paired up. Therefore, in a low-symmetry CF the energy levels of the Kramers ions are split into doubly degenerate states (Kramers doublets), while the energy levels of non-Kramers ions are split into non-degenerate or singlet states. Thus, the symmetry of the crystal field (CF) acting on the RE-ions will define both their energy and Wave functions symmetry characteristics in the condensed medium.

§1.2. Paramagnetism of the "free" RE-ions.

Let us consider the interaction between the "free" RE-ion (as defined in Sec. 1.1) with an external magnetic field *H.* An interaction Hamiltonian of the ion with an external magnetic field (denoted the Zeeman Hamiltonian) is usually written as,

$$\hat{H}_Z = \mu_B\left(\hat{L} + 2\hat{S}\right)\vec{H} = \mu_B(\hat{J} + \hat{S})\vec{H} \,. \qquad (1.6)$$

If the field H is directed along the *z*-axis of the coordinate system, the Hamiltonian can be written in the following form,

$$\hat{H}_Z = \mu_B(\hat{J}_Z + \hat{S}_Z)H \,. \qquad (1.7)$$

Based on the state wave functions, $|LSJM_J>$, that are distinct for each state, we can write the matrix elements for this Hamiltonian as [3],

$$< LSJM_J \,|\, \hat{H}_Z \,|\, LSJM_J >= g_J \mu_B M_J H \ , \qquad (1.8)$$

where $g_J = 1 + \dfrac{J(J+1) + S(S+1) - L(L+1)}{2J(J+1)}$ is the Lande' factor for the multiplet of the RE-ion,

and

$$< LS(J+1)M_J \,|\, \hat{H}_Z \,|\, LSJM_J >= -g'_J \mu_B H\left[(J+1)^2 - M_J^2\right]^{1/2} \qquad (1.9)$$

where $g'_J = \left[\dfrac{(J+L+S+2)(L-J+S)(J-L+S+1)(J+L-S+1)}{4(J+1)^2(2J+1)(2J+3)}\right]^{1/2}$.

Let us consider now the behavior of an ensemble of free RE-ions in an external magnetic field. In this case, the magnetic field tends to orient the magnetic moments $\vec{M}$ of the ions, whereas the thermal motion tends to disorient them. As $\vec{M}$ is spatially quantized, the energy of the interaction between the magnetic moment $\vec{M}$ of the RE ion with the magnetic field must also be quantized. This additional interaction energy W_H is given by the expression,

$$W_H = -g_J M_J \mu_B H . \qquad (1.10)$$

As the projection M_J of the angular momentum $\vec{J}$ takes on $(2J + 1)$ values, with $-J \le M_J \le J$, W_H splits the (initially degenerate) energy level (multiplet) of the ion into sublevels located above and below the unperturbed energy level. These sublevels are equally spaced in the energy spectrum, with the energy separation between the magnetic (or Zeeman) sublevels equal to $\Delta_H = g_J \mu_B H$.

The magnetization of N ion ensembles, each having similar equidistant structure in the energy spectrum, is isotropic and can be represented as [3,11],

$$I = I_0 B_J(x), \qquad (1.11)$$

where $B_J(x)$ is the Brillouin function [11],

$$B_J(x) = \frac{2J+1}{2J}\coth\left(\frac{2J+1}{2J}x\right) - \frac{1}{2J}\coth\left(\frac{1}{2J}x\right) \qquad (1.12)$$

and $x = \frac{g_J \mu_B JH}{kT}$. In eqn. (1.11), $I_0 = Ng_J \mu_B J$ is the saturation magnetization of N ion ensembles at $T = 0$ K (for example, for the RE-ion Gd^{3+}, $I_0 = 7\mu_B$).

Keeping only the first terms in the series expansions of the coth(x) terms in eqn. (1.12) allows us to simplify eqn. (1.11) for high T and a low H (i.e., x <<1) as,

$$I = \frac{NJ(J+1)g_J^2 \mu_B^2}{3kT} H , \qquad (1.13)$$

where k is the Boltzmann constant. I corresponds to the expression for the paramagnetic susceptibility χ, which can be written as,

$$\chi = \frac{C}{T} , \qquad (1.14)$$

where C is the Curie constant[1] $C = \frac{NJ(J+1)g_J^2\mu_B^2}{3k} = \frac{NM_J^2}{3k}$, and M_J is the atomic magnetic momentum. Expression (1.14) is called the Curie law, and this expression is used in this text for several compounds in which the RE-ions can be considered as free ions. For the most part, rare-earth compounds obey the Curie-Weiss law [3,11,12],

$$\chi = \frac{C}{T - \theta_p} \ , \qquad (1.15)$$

where θ_p is the Weiss constant, often called the paramagnetic or Curie temperature [10], which takes into account both magnetic and electric interactions between magnetic ions in paramagnets.

In addition to the orientation-dependent paramagnetism just described, we also encounter Van-Vleck paramagnetism, caused by the mixing of wave functions of closely spaced electronic states of certain RE-ions by an external magnetic field H. This situation is especially common in compounds containing the RE-ions Eu^{3+} and Sm^{3+} [3,12].

---

[1] If the number of ions N equals Avogadro's number N_A, then we can write [11]: $C = \frac{N_A J(J+1)g_J^2\mu_B^2}{3k} = \frac{1}{8}g_J^2 J(J+1)$ and the magnetic susceptibility χ_m (calculated on the basis of one mole) is: $\chi_m(cm^3) = \frac{1}{8T}g_J^2 J(J+1)$. We can also write the specific χ magnetic susceptibility (calculated on the basis of one gram) as: χ (cm^3/gram) $= \frac{\chi_m}{M}$, where M is the molecular weight. In addition, the magnetic susceptibility χ_V calculated based on a unit of volume (cm^{-3}) is: $\chi_V = \frac{\rho\chi_m}{M}$, where ρ is the density (in gram/cm^3). In this way we see that χ_V *is a dimensionless quantity*! Therefore, the magnetization M_V that is calculated on the basis of a unit of volume (cm^{-3}) has identical dimensionality to the external magnetic field H. But in this case, the magnetization M_V can be expressed in units of *Gauss* (gs), whereas the dimensionality of the external magnetic field is in units of *Oersted* (Oe).

§1.3. The theory of the rare-earth ions optical properties in the condensed medium

Optical properties of rare-earth compounds: The optical properties of rare-earth (RE) compounds are characterized primarily by electric-dipole (ED) and magnetic-dipole (MD) transitions between electronic energy levels of the positively charged RE ions. Multiplet levels of the $4f^n$ electronic configuration, degenerate in the free ion, are split by the electrostatic field (Stark effect) produced by the ligand environment of the ion, according to the site symmetry at the host site. Valence shell 4*f* electrons of the RE-ion are mostly shielded from the effects of the ligands by the filled 5*s* and 5*p* orbitals, which accounts for the detailed and complex character of the ion energy spectrum. Both electric and magnetic moments of the RE-ion participate in the ion interaction with an incoming electromagnetic wave. Interactions of moments of higher orders (e.g. the electric quadrupole) with the incoming light are generally very weak and for that reason are not considered here.

Intra-configurational transitions between $4f^n$ states must have even parity, as the initial and final states have the same parity. By contrast, inter-configurational transitions between $4f^n$ and $4f^{n-1}5d$ states must have odd parity. As the electric dipole (ED) operator has odd parity, and the magnetic dipole (MD) operator has even parity, only the MD participates in intra-configurational $4f^n$ transitions in the free ion. However, if the RE-ion is located in a non-centrosymmetric crystalline (ligand) environment, then odd-parity contributions from the crystal field can produce a parity-mixing of the $4f^n$ electronic states, allowing the ED interaction to participate. Because of the limited selection rules for the MD interaction, the rich spectra for RE-ions is dominated by the ED interaction, assisted by the non-centrosymmetric crystal field, which solves Van-Vleck's "puzzle of rare-earth spectra in solids" [13]. If the RE-ion is located in a centrosymmetric crystalline environment, ED transitions between the $4f^n$ electronic states remain forbidden, however, ED transitions may still be observed via coupling with odd-parity vibronics [14,15].

In the first approximation, the RE-ion interaction with its ligand environment is considered electrostatically, with the electric field of the surrounding ions considered simply as point electric (usually negative) charges. In this ligand environment, the RE-ion spectra reveal a shift in energy relative to the "free ion" energy levels due to the effects of the crystalline electric field and possibly other lattice and magnetic perturbations. Since the $4f^n$ electrons are strongly localized near the ion core and are electrostatically screened by the filled 5*s* and 5*p* electron shells, the interaction of the crystal field (CF) acting on the $4f^n$ electrons is relatively small (on the order of ~ 10^2 cm^{-1}) [3]. On the other hand, the spin-orbit interaction acting upon the $4f^n$ electrons is approximately an order of magnitude larger. This means that the CF splitting of the Stark levels within each ${}^{(2S+1)}L_J$ multiplet is generally small compared to the energy separations between the $4f^n$ multiplets. According to the Lande' rule, these energy separations are given by $\Delta E_J = (J+1)\xi$, where ξ is the spin-orbit constant and *J* is the total angular momentum. Hence, although the CF interaction produces some *J*-mixing of the Stark levels, from a physical point of view, *J* may still be used as an approximate quantum number.

Because of the parity-forbidden nature of the transitions, the intensities of the $4f^n \rightarrow 4f^n$ electric-dipole transitions are 10^4–10^6 smaller than for the ED-allowed $4f^n \rightarrow 4f^{n-1}5d$ transitions. Based on these observations and the results presented earlier in Chapter 1 for RE free ions (see §1.1), we see that the absorption spectra of RE-compounds contains sharp absorption lines representing transitions inside the $4f^n$ electronic shell in the visible and infrared spectral range, and that very strong absorption bands associated with inter-configurational $4f^n \rightarrow 4f^{n-1}5d$ transitions are observed in the ultra-violet (UV) spectral range [16-18]. Absorption bands associated with the allowed $4f^n \rightarrow 4f^{n-1}5d$ transitions typically have line widths in the range ~ $10^2 \div 10^3$ cm^{-1} which strongly depend on the symmetry of the crystalline environment of the RE-ion, since the excited 5*d* electron has a much greater interaction with the ligand environment compared to the "shielded" 4*f* electrons [18].

Optical absorption bands associated with the ED-allowed $4f^n \rightarrow 4f^{n-1}5d$ ($f \rightarrow d$) transitions are observed for a number of trivalent RE-ions in different crystalline hosts [19-22]. The smallest energy separations between the ground $4f^n$ and excited $4f^{n-1}5d$ configurations occurs for the Pr^{3+}, Nd^{3+}, Ce^{3+} and Tb^{3+} ions, allowing the $f \rightarrow d$ bands of absorption and luminescence for these ions to be observed within the transparency range of a wide class of crystalline hosts. For other RE-ions, the $f \rightarrow d$ transitions are observed much further into the UV.

Selection rules for the ED- and MD-transitions: Selection rules (or transition rules) in quantum mechanics formally limit the allowed transitions in the atomic system from one quantum state to another [23]. The selection rules in the optical spectra follow from various laws of conservation of physical values: the conservation of impulse momentum, its quantization axis projection, the conservation of parity, and so on. Selection rules for the quantum number J are connected with a change in the ion impulse momentum at the emission of a photon, $\Delta J = \pm 1$. As J is the vector sum of $L + S$, the change of quantum number J can be connected either with a change in S or L. Electric-dipole (ED) transitions do not change the value of the spin angular momentum, S. Similarly, magnetic-dipole (MD) transitions do not change the value of the orbital angular momentum, L. Therefore ED-transitions arising in the free RE ion between quantum states of opposite parity are connected with changes of the quantum numbers S, L, and J in the following way,

$$\Delta S = 0,\ \Delta L = 0, \pm 1, \text{ and } \Delta J = 0, \pm 1$$

(transitions from $J = 0$ to $J' = 0$ excluded). The ED transitions arising between quantum states of the same parity are "forbidden" due to the fact that an odd-parity ED operator cannot connect two states of like parity. However, when the ion lies in a non-centrosymmetric site in the crystalline lattice, odd rank terms in the crystal-field Hamiltonian can cause parity-mixing of the initial and final states, allowing "forced" ED transitions. The quantum number selection rules for these forced ED transitions then becomes,

$$\Delta S = 0,\ \Delta L \leq 6, \text{ and } \Delta J \leq 6.$$

Similarly, MD-transitions arising in the free RE ion between quantum states of the same parity are connected with changes of the quantum numbers *S*, *L,* and *J*, as,

$$\Delta S = 0,\ \Delta L = 0, \text{ and } \Delta J = 0, \pm 1$$

(transitions from $J = 0$ to $J = 0$ excluded). The *S*, *L*, and *J* are the corresponding spin angular momentum, orbital angular momentum, and total angular momentum for the multi-electron $4f^n$ system. MD-transitions are allowed in both centrosymmetric and non-centrosymmetric point group symmetry. However, transitions allowed by the magnetic-dipole mechanism are rare, because of the selection rule $\Delta J = 0$ or $\Delta J = \pm 1$ (but not $0 \leftrightarrow 0$). The best-known MD-transitions are for transitions $^7F_1 \rightarrow {}^5D_0$ and $^7F_0 \rightarrow {}^5D_1$ of Eu^{3+}.

Judd-Ofelt theory: The optical spectra of the trivalent rare-earth ions in different hosts, including the glasses [24], to mention a few, display a wealth of numerous transitions at relatively low energies of excitation (<40000 cm^{-1}). These spectra are due to $4f \rightarrow 4f$ transitions that are forbidden in the electric-dipole approximation, based on the requirement of a change in parity in the transition. However, Judd [25] and Ofelt [26] proposed mixing states of opposite parity in the wavefunctions for these transitions through the odd terms in the crystal-field Hamiltonian that arise when the ion lies at a non-centrosymmetric site [27].

The crystal field removes some, or for certain RE^{3+} ion, all the degeneracy associated with the total angular momentum quantum number, *J*, split by the crystal field. The crystal-field splitting wavefunctions, based on the even-terms of the $4f^n$ Hamiltonian only, represented as the initial $|i>$ and final $|j>$ states, are constructed from the same $4f^n$ configuration and therefore possess the same parity. Thus, the electric-dipole (ED) operator for a many-electron system, namely,

$$\vec{D} = e\sum_{i=1}^{n} \vec{r}_i\,, \qquad (1.16)$$

cannot connect states within the same configuration, and we have as a first approximation, $< i | \vec{D}^{(1)} | j >= 0$. This is merely a consequence of the well-known Laporte rule. To obtain non-vanishing matrix elements for the components of $\vec{D}^{(1)}$, however, it is necessary to admix into $| i >$ and $| j >$ states that are built from configurations that have opposite parity to the $4f^n$. One of the most important mechanisms for this mixing is the coupling of states of opposite parity (for example, $4f^{n-1}5d$ or $4f^{n-1}5g$) by the odd terms in the crystal field potential or crystal-field Hamiltonian, $\hat{H}_{CF} = -eV_{CF}$., which is generally expressed in terms of the spherical coordinates $(r_i, \theta_i, \varphi_i)$ of electron i,

$$V_{odd} = \sum_{\substack{t=3,5,7 \\ p=2,4,6 \\ p<t}} A_{tp} D_p^{(t)} \qquad (1.17)$$

$$D_p^{(t)} = \sum_i r_i^t \sqrt{\frac{4\pi}{(2t+1)}} \cdot Y_{tp}(\theta_i, \varphi_i),$$

where, $(A_{tp})^* = A_{t,-p}$ and Y_{tp} are spherical harmonic operators, with the sum being over the individual electrons of the system. The ED moment of a given electron can be represented as,

$$D_q^{(1)} = \sum_i r_i \sqrt{\frac{4\pi}{3}} \cdot Y_{1q}(\theta_i, \varphi_i), \qquad (1.18)$$

where $q = 0, \pm 1$, and represents the polarization of the incident light.

The A_{tp} coefficients in Eqn. (1.17) depend on the symmetry of the host crystal lattice. For example, when the site symmetry of the RE-ion is D_2 (e.g., the garnets), the odd terms in the crystal field potential are given by the following expression [28],

$$\begin{aligned} V_{odd} &= A_{32}(D_2^{(3)} - D_{-2}^{(3)}) + A_{52}(D_2^{(5)} - D_{-2}^{(5)}) + A_{54}(D_4^{(5)} - D_{-4}^{(5)}) \\ &+ A_{72}(D_2^{(7)} - D_{-2}^{(7)}) + A_{74}(D_4^{(7)} - D_{-4}^{(7)}) + A_{76}(D_6^{(7)} - D_{-6}^{(7)}) \end{aligned} \qquad (1.19)$$

This particular theoretical description of the strengths of the parity-forbidden (ED) transition was established by Judd [25] and Ofelt [26]. The matrix elements of the $D_q^{(1)}$ operator are given by,

$$< f^n \phi J M \mid D_q^{(1)} \mid f^n \phi' J' M' >= \sum_{\substack{\lambda=2,4,6 \\ p,t}} (2\lambda+1)\cdot(-1)^{p+q+J-M} \begin{pmatrix} J & \lambda & J' \\ -M & p+q & M' \end{pmatrix} \cdot \begin{pmatrix} 1 & \lambda & t \\ q & -p-q & p \end{pmatrix} A_{tp}\, \Xi(t,\lambda) \cdot \quad (1.20)$$

$$\cdot < f^n \phi J \| U^{(\lambda)} \| f^n \phi' J' >$$

The parameters $\Xi(t,\lambda)$ represent the $4f \rightarrow 4f$ transition intensity in the Judd-Ofelt theory and have a following form,

$$\Xi(t,\lambda) = 2(2l+1)\sum_{l'} (2l'+1)(-1)^{l+l'} \begin{Bmatrix} 1 & \lambda & t \\ l & l' & l \end{Bmatrix} \begin{pmatrix} l & 1 & l' \\ 0 & 0 & 0 \end{pmatrix} \begin{pmatrix} l' & t & l \\ 0 & 0 & 0 \end{pmatrix} \frac{< nl \mid r \mid n'l' >< nl \mid r^{(t)} \mid n'l' >}{(E_{n'l'} - E_{nl})}. \quad (1.21)$$

where in expressions (1.20) and (1.21), the $\begin{pmatrix} j_1 & j_2 & j_3 \\ m_1 & m_2 & m_3 \end{pmatrix}$ are 3*j*-symbols [25,26]; $\begin{Bmatrix} a & b & c \\ l & k & m \end{Bmatrix}$ is the 6*j*-symbol connecting symmetry elements [25,26]; J' and J are the total angular momenta of the excited and ground multiplets of the RE^{3+} that are connected by the ED $4f \rightarrow 4f$ transition; M' and M are their projections; λ = 2,4,6 are the transitional moments in the Judd-Ofelt theory [25,26]; $t = \lambda \pm 1$, p are the indexes of the odd spherical harmonics [25,26]; and $< f^n \phi J \| U^{(\lambda)} \| f^n \phi' J' >$ are the reduced matrix elements of the $4f \rightarrow 4f$ transition tabulated in [25].

For our calculations, l = 3 (*f*) and l' = 2 (*d*) or 4 (*g*) are the orbital moments for one-electron systems of opposite parity; $<nl|r|nl'>$ is the radial integral; $E_{nl'}$ and E_{nl} are the energies of the mixing states (by the odd components of the crystalline electrostatic potential, V_{odd}) of the RE-ion. The other notations used in eqns. (1.20) and (1.21) are the same as given in Ref. [25]. In deriving the above expressions, the summations over all the perturbing states are made by making the approximation of replacing the energy denominators by a single denominator $\Delta(nl', nl)$, followed by making closure over the perturbing states. Although this "closure approximation" may lead to substantial uncertainty in the calculations, this approximation is a valid starting point for perturbation expansions, where the energy denominator differences are accounted for in the higher-order terms of the perturbation expansion.

Following Condon and Shortley [29] we can define the "line strength" $S(a,b)$ between the two levels a and b as,

$$S(a,b) = \sum_{\alpha\beta} |< \alpha |\hat{A}| \beta >|^2 , \tag{1.22}$$

where $\hat{A}$ may be either the electric $\hat{D}$, or magnetic $\hat{M}$ dipole moment operator, and α and β are the components of states a and b, respectively. The magnetic-dipole moment (MD), and the electric-dipole moment (ED) operators for the many-electrons system are given by,

$$\hat{M} = -\frac{e}{2mc}(\hat{L} + 2\hat{S}), \qquad \hat{L} = \sum_i l_i \quad \text{and} \quad \hat{S} = \sum_i s_i$$

and $$\hat{D} = \sum_i \hat{d}_i , \qquad \hat{d}_i = -e\hat{r}_i \tag{1.23}$$

respectively, where e is the electron charge and m is its mass, the subscript i is summed over the electrons, and $\hat{l}$ and $\hat{s}$ are single-electron operators are expressed in units of $\hbar$.

We adopt here the irreducible tensor description given by Racah [30] and follow by using the tensor set of the components of a vector (or first rank tensor) $\vec{A}$ as given by [30],

$$\begin{aligned} A_0^{(1)} &= A_z = | A | C_0^{(1)} \\ A_{+1}^{(1)} &= -\frac{1}{\sqrt{2}}(A_x + iA_y) = | A | C_{+1}^{(1)} \\ A_{-1}^{(1)} &= \frac{1}{\sqrt{2}}(A_x - iA_y) = | A | C_{-1}^{(1)} , \end{aligned} \tag{1.24}$$

where $C_q^{(1)}$ is a spherical tensor operator (q = 0, ±1) normalized like the Legendre polynomials [30]. In this notation the eqns. given in (2.9) become,

$$\hat{M}_q^{(1)} = \sum_i (\hat{L}_{iq}^{(1)} + 2\hat{S}_{iq}^{(1)}) \text{ , and}$$

$$\hat{D}_q^{(1)} = \sum_i r_i C_{iq}^{(1)} ,$$

and the line strength for a transition between the α and β components of states a and b can be written as,

$$S(\alpha,\beta) = \sum_q |< \alpha |A_q^{(1)}| \beta >|^2 = |< \alpha | A_{+1}^{(1)} | \beta >|^2 + |< \alpha | A_{-1}^{(1)} | \beta >|^2 + |< \alpha | A_0^{(1)} | \beta >|^2 , \tag{1.25}$$

where $A^{(1)}$ may be either $M^{(1)}$ or $D^{(1)}$.

Let us now consider the line strength for the transition from multiplet (LSJ) to the multiplet ($L'S'J'$) within the $4f^n$ configuration. For this purpose, we can rewrite eqn. (1.20) in a more compact form as,

$$< LSJ,M \mid \hat{D}_q^{(1)} \mid L'S'J',M' >= \sum_{p,\lambda} (-1)^{(J-M)} \begin{pmatrix} J & \lambda & J' \\ -M & p+q & M' \end{pmatrix} < LSJ \parallel U^{(\lambda)} \parallel L'S'J' > \varphi_{pq}^{(\lambda)} \ , \tag{1.26}$$

where,

$$\varphi_{p,q}^{(\lambda)} = \sum_t (2\lambda+1) \cdot A_{tp} \Xi(t,\lambda) \cdot (-1)^{p+q} \begin{pmatrix} 1 & \lambda & t \\ q & -p-q & p \end{pmatrix} \ . \tag{1.27}$$

Now we can write the following expression for the line strength for this transition as,

$$S = \sum_{a,b,q} |< a \mid \hat{D}_q^{(1)} \mid b >|^2 = \sum_{qMM'} |< LSJ,M \mid \hat{D}_q^{(1)} \mid L'S'J',M' >|^2 \ . \tag{1.28}$$

We can now find the square of the matrix element given in eqn. (1.28) and obtain the following expression by taking into account that the index q and the momentum projections M, M' are fixed so that,

$$\begin{aligned} |< LSJ,M \mid \hat{D}_q^{(1)} \mid L'S'J',M' >|^2 = e^2 \sum_{\lambda\lambda' pp' tt'} (2\lambda+1)(2\lambda'+1) \cdot (-1)^{2J-2M} \begin{pmatrix} J & \lambda & J' \\ -M & p+q & M' \end{pmatrix} \begin{pmatrix} J & \lambda' & J' \\ -M & p'+q & M' \end{pmatrix} \cdot \\ \cdot A_{t'p'} A_{tp} \begin{pmatrix} 1 & \lambda & t \\ q & -p-q & p \end{pmatrix} \begin{pmatrix} 1 & \lambda' & t' \\ q & -p'-q & p' \end{pmatrix} \Xi(t,\lambda) \Xi(t',\lambda') < LSJ \parallel U^{(\lambda)} \parallel L'S'J' >< LSJ \parallel U^{(\lambda')} \parallel L'S'J' > \end{aligned} \tag{1.29}$$

At the fixed values of q, M, and M' we have an obvious equality, $p = p'$, which follows from the property of 3j-symbols [29] that the sum of projections ($m_1 + m_2 + m_3$) = 0. Now we can sum eqn. (1.29) over the momentum projections M, M', (p+q), and q indices as follows,

$$\begin{aligned} \sum_{\substack{qMM_o \\ p+q}} |< LSJ,M \mid \hat{D}_q^{(1)} \mid L'S'J',M' >|^2 = e^2 \sum_{\substack{\lambda\lambda'(p+q)tt' \\ qMM_o}} (2\lambda+1)(2\lambda'+1) \cdot (-1)^{2J-2M} \begin{pmatrix} J & \lambda & J' \\ -M & p+q & M' \end{pmatrix} \begin{pmatrix} J & \lambda' & J' \\ -M & p+q & M' \end{pmatrix} \cdot \\ \cdot A_{t'p} A_{tp} \begin{pmatrix} 1 & \lambda & t \\ q & -p-q & p \end{pmatrix} \begin{pmatrix} 1 & \lambda' & t' \\ q & -p-q & p \end{pmatrix} \cdot \Xi(t,\lambda) \cdot \Xi(t',\lambda') < LSJ \parallel U^{(\lambda)} \parallel L'S'J' >< LSJ \parallel U^{(\lambda')} \parallel L'S'J' > \end{aligned} \tag{1.30}$$

Eqn. (1.30) can be simplified by using the orthogonality conditions,

$$\sum_{MM_o}\begin{pmatrix} J & \lambda & J' \\ -M & p+q & M' \end{pmatrix}\begin{pmatrix} J & \lambda' & J' \\ -M & p+q & M' \end{pmatrix} = \frac{1}{(2\lambda+1)}\delta_{\lambda\lambda'}$$

and, $$\sum_{q,(p+q)}\begin{pmatrix} 1 & \lambda & t \\ q & -p-q & p \end{pmatrix}\begin{pmatrix} 1 & \lambda & t' \\ q & -p-q & p \end{pmatrix} = \frac{1}{(2t+1)}\delta_{tt'}$$

that follow from the general orthogonality rule for 3*j*-symbols [29],

$$\sum_{m_1 m_2}\begin{pmatrix} j_1 & j_2 & j \\ m_1 & m_2 & m \end{pmatrix}\begin{pmatrix} j_1 & j_2 & j' \\ m_1 & m_2 & m' \end{pmatrix} = \frac{1}{(2j+1)}\delta_{jj'}\delta_{mm'} \quad .$$

Eqn. (1.30) then becomes,

$$\sum_{\substack{M,M_0,q,\\(p+q)}} |< LSJ,M \mid \hat{D}_q^{(1)} \mid L'S'J',M' >|^2 = e^2(2\lambda+1)\cdot |< LSJ \parallel U^{(\lambda)} \parallel L'S'J' >|^2 \cdot \sum_{t,p} |A_{tp}|^2 \cdot \frac{\Xi^2(t,\lambda)}{(2t+1)} \quad . \qquad (1.31)$$

Now the expression for the line strength in the Judd-Ofelt approximation for ED transitions, S_{ed}, which is proportional to the square of the matrix elements $< f^n\phi J \parallel U^{(\lambda)} \parallel f^n\phi' J' >$ can be written as,

$$S_{ed} = e^2 \sum_{\lambda=2,4,6} \Omega_\lambda \cdot |< LSJ \parallel U^{(\lambda)} \parallel L'S'J' >|^2 , \qquad (1.32)$$

where $\Omega_\lambda = (2\lambda+1)\sum_{t,p} |A_{tp}|^2 \cdot \frac{\Xi^2(t,\lambda)}{(2t+1)}$ are the Judd-Ofelt parameters [25,26].

The Ω_λ parametrization is the most general one-electron, spin-independent scheme possible. For integrated multiplet-to-multiplet intensities, this parametrization scheme has been applied successfully to rationalize experimental results for hundreds of data sets [31].

Similarly, the $A_{tp}\Xi(t,\lambda)$ parameters may be used directly [32] to calculation transition intensities between individual crystal-field (Stark) levels within each multiplet. For simplicity, a new parameter, $A_{tp}^{\lambda} = \frac{(2\lambda+1)}{\sqrt{2t+1}} A_{tp}\Xi(t,\lambda)$ is commonly defined, giving the following identification with the Judd-Ofelt parameters,

$$\Omega_\lambda = \frac{1}{(2\lambda+1)}\sum_{t,p} |A_{tp}^{\lambda}|^2 \ , \qquad (1.33)$$

In practice, the A_{tp}^{λ} parametrization is more general then the $A_{tp}\Xi(t,\lambda)$ definition given above, because the $\Xi(t,\lambda)$ implicitly assume separability of the individual

ligand-metal interactions (commonly called the "superposition model" approximation), and thus ignores possible contributions from other sources, such as ligand polarizability [32]. Additional parameters with $t = \lambda$ are included in the most general A_{tp}^{λ} calculation, giving the following reduced restrictions: $\lambda = 2, 4, 6$; $t = \lambda-1, \lambda, \lambda+1$; and $p \leq t$ is restricted by the group theoretical rules determined by the site symmetry of the RE-ion [31].

The Judd-Ofelt intensity parameters are found by experimental methods. Extensive reviews have also been reported by Weber [33] and Carnall [34]. The wide application of the Judd-Ofelt parameters Ω_λ in the optical spectroscopy of RE-ions in crystals has been greatly assisted by the definite character of the doubly-reduced tensor operators $< f^n \phi J \| U^{(\lambda)} \| f^n \phi' J' >$, which are generally taken to be host invariant [34]. The Judd-Ofelt parameters Ω_λ ($\lambda = 2, 4, 6$), for a given rare-earth ion – host combination, are determined from eqn. (1.33) by fitting the observed oscillator strengths f for the integrated multiplet-to-multiplet transition from (LSJ) to ($L'S'J'$), written as,

$$f(LSJ;L'S'J') = \frac{2m\omega_{JJ'}}{3\hbar(2J+1)e^2\bar{n}^2}\chi_{ed}S_{ed}\,, \tag{1.34}$$

where $\bar{n}$ is the mean refractive index and χ_{ed} is the Lorentz correction for the RE-ion at the wavelength of the absorption representing the transitions between the manifolds. For ED transitions, $\chi_{ed} = \frac{\bar{n}(\bar{n}^2+2)^2}{9}$.

Once the Judd-Ofelt parameters are determined, they can be used to calculate the oscillator strengths, and other transition properties between ground and excited states of the RE-ion in condensed medium. For instance, the spontaneous relaxation rate A corresponding to an ED transition from the multiplet (LSJ) to the multiplet ($L'S'J'$) can be related to the line strength by the expression,

$$A(LSJ;L'S'J') = \frac{32\pi^3}{3\hbar(2J_0+1)\lambda^3}\chi_{ed}S_{ed}(LSJ;L'S'J')\,. \tag{1.35}$$

The radiative lifetime of a multiplet, τ_{rad}, is related to the radiative decay rate through,

$$\frac{1}{\tau_{rad}} = \sum_{J} A(J;J'), \tag{1.36}$$

where the summation is over multiplets of energy lower than the radiative level.

Since magnetic dipole radiation is also observed in the optical spectra of the RE compounds, it is also necessary to calculate matrix elements of the magnetic dipole operator, $\hat{M} = \mu_B \sum_i (\hat{l}_i + 2\hat{s}_i) = \mu_B (\hat{L} + 2\hat{S})$. This is straightforward, since the MD operator connects states of the same parity. Thus, the matrix elements of the MD operator can be written as [25,26,29,31],

$$< a \mid \hat{M}_q \mid b >= \mu_B < LSJ, M \mid (\hat{L} + 2\hat{S})_q \mid L'S'J', M' >= \mu_B \delta_{LL'} \delta_{SS'} (-1)^{J-M} \begin{pmatrix} J & 1 & J' \\ -M & q & M' \end{pmatrix}$$
$$\times < LSJ \parallel \hat{L} + 2\hat{S} \parallel L'S'J' > \tag{1.37}$$

where $\mid a >$ and $\mid b >$ are the initial and final $4f^n$ states and μ_B is the Bohr magneton. As an example, in Eu^{3+} ion MD transitions between states ^5D_J and ^7F_J are prohibited since these transitions involve $\Delta L = 1$ and $\Delta S = 1$. However, due to the spin-orbit interaction, the wavefunctions of the ^5D_J and ^7F_J multiplets are mixed, leading to the appearance of MD-transitions between these states.

Explicit expressions of the reduced matrix elements in an *SLJ* scheme are given by Condon and Shortley [29] and have the following form,

$$< LSJ \parallel \hat{L} + 2\hat{S} \parallel LSJ >= \hbar \left(1 + \frac{J(J+1) + S(S+1) - L(L+1)}{2J(J+1)} \right) \cdot \sqrt{J(J+1)(2J+1)} \tag{1.38}$$

$$< LSJ \parallel \hat{L} + 2\hat{S} \parallel LS(J-1) >= \hbar \frac{\sqrt{\left[(S+L+1)^2\right] \cdot \left[J^2 - (L-S)^2\right]}}{2\sqrt{J}} \tag{1.39}$$

$$< LSJ \parallel \hat{L} + 2\hat{S} \parallel LS(J+1) >= \hbar \frac{\sqrt{\left[(J+1)^2 - (S-L)^2\right] \cdot \left[(L+S+J+2)(S+L+J)\right]}}{2\sqrt{J+1}} \tag{1.40}$$

Note that the radiative MD transition probability between states *a* and *b* can be determined by the following expression,

$$A(a,b) = \frac{4\omega^3 \bar{n}^3 \mu_B^2}{3\hbar c_3} \cdot \sum_{a,b,q} \frac{|< a \mid \hat{M}_q \mid b >|^2}{(2J+1)}, \tag{1.41}$$

where $\bar{n}$ is the index of refracton and (2J + 1) is the order of degeneracy of the initial state of the radiative transition.

It is important to note that the expression given in eqn. (1.31) for the matrix elements of the parity-forbidden ED $4f \rightarrow 4f$ transition can be used successfully for the calculations of the oscillator strengths (or line strengths) between Stark sublevels of the ground and excited multiplets of the RE-ion in the condensed medium (including rare-earth paramagnetic glasses [24]).

§1.4. Optical properties of the rare-earth paramagnetic glasses

The spectroscopic properties of the rare-earth paramagnetic glasses (including fluoride glasses doped by RE-ions) have been studied extensively during the past two decades [ ]. However most studies are however restricted to optical absorption and luminescence data. Only a few MCD studies of lanthanide ions in vitreous matrices have been reported until now: *Boccara* [ ] investigated the MCD of Eu^{3+} ions in barium-crown glass. *Collocott et al.* studied the magneto-optical properties of Er^{3+} [ ], Pr^{3+} [ ] and Ho^{3+} [ ] in soda glass. *Valiev et al.* [ ] and *Klochkov et al.* [ ] have published the MCD spectra of Er^{3+} doped phosphate glass. *Binnemans et al.* [ ] recently have studied the magnetic circular dichroism spectra of Eu^{3+} in fluorophosphate glass [ ]. Also in the next paper *Binnemans et al.* [ ], they reported the magnetic circular dichroism (MCD) and optical absorption spectra of a Pr^{3+} ions doped to the fluorozirconate (ZBLAN) glass. They noted that the advantage of a glass matrix over a solution is that the magnetoopiical properties of randomly oriented lanthanide systems can be studied also at low temperatures. In addition to the MCD spectra, the optical absorption spectra have been recorded too. The intensities of the 4f→4f induced electric dipole transitions have been parametrized in terms of three Judd-Ofelt intensity parameters.

Absorption spectra of fluorozirconate (ZBLAN) glass doped by Pr^{3+} ions recorded by *Binnemans et al.* [ ] on an AVIV 17DS spectrophotometer in the 400-2500 nm range. The MCD spectra were recorded on an AVIV 62DS circular dichroism spectrometer, extended with an electromagnet (Oxford Instruments). The magnetic field strength was 0.9 Tesla {9000 Gauss). The wavelength range for the

MCD measuremente was 400-650 nm. The spectral band width for both the absorption and MCD spectra was 0.10 nm. Spectra of ZBLAN:Pr^{3+} (1%) have been recorded at the different temperatures between 4.2 K and room-temperature. The room-temperature (293 K) absorption spectra of ZBLAN:Pr^{3+} in [ ] was recorded between 15000 and 25000 cm^{-1}. The transitions were assigned by comparing the band positions in absorption spectrum with the energy level scheme of LaF_3:Pr^{3+}, published by *Carnall et al.* [ ]. All transitions, in the absorption spectrum of Pr^{3+} start from the $^3H_4$ ground state. The spectral transitions can be divided into four groups: transitions to the $^3H_6$, $^3F_2$, $^3F_3$ and $^3F_4$ manifolds in the infrared spectrum, the weak transition to the $^1G_4$, state at 9895 cm^{-1}, the $^3H_4 \rightarrow {}^1D_2$ transition at 17024 cm^{-1} and the complex group of the transitions to the $^3P_0$, $^3P_1$, $^3P_2$ and $^1I_6$ manifold in the violet-blue region. The latter group is responsible for the green color of Pr^{3+} ion. The $^3P_1$ and the $^1I_6$ overlap and cannot be even resolved at low temperatures. At cryogenic conditions the $^3P_2$ levels show distinct crystal-field splitting.

The dipole strengths of the 4f→4f transitions were determined by integrating the absorption bands and using the expression [ ]:

$$D = \frac{1}{108{,}9 \cdot C \cdot d} \int \frac{A(\nu)}{\nu} d\nu \qquad (1.42)$$

where D is the dipole strength (in Debye^2), C is the concentration of the lanthanide ion (in mol/L) and d is the sample thickness (in cm). The concentration of Pr^{3+} ions is 0,3166 mol/L. It is assumed that all ions are in the $^3H_4$ ground stale at ambient temperature, so that the Boltzmann population factor is unity. Notice that for oriented systems (e.g., single crystals), the definition of the dipole strength contains an additional factor 1/3 in the right hand side of equation (1.42) [ ]. The dipole strength D is related to the often used oscillator strength (dimensionless):

$$D = \frac{2{,}127 \cdot 10^6 \cdot f}{\nu_0} \qquad (1.43)$$

where ν_0 (in cm^{-1}) is the barycenter of the absorption band.

According to the Judd-Ofelt theory [ ] the dipole strength D of an induced electric dipole transition is:

$$D = \frac{10^{36}}{g_a} \cdot \frac{(n^2+2)^2}{9n} \cdot e^2 \sum_{\lambda=2,4,6} \Omega_\lambda \cdot / < \Psi // U^{(\lambda)} // \Psi' > /^2 \qquad (1.44)$$

where $\Omega_\lambda (\lambda = 2,4,6)$ are the phenomenological Juudd-Ofelt intensity parameters which have to be determined by a least-squares fit of the experimental data. The $/ < \Psi // U^{(\lambda)} // \Psi' > /^2$ are squared reduced matrix elements between the ground state Ψ and the excited state Ψ', and U is the unity tensor operator. The reduced matrix elements are relatively insensitive to the environment and can be considered as constants for a given lanthanide ion. We used the reduced matrix elements reported by *Carnall et al.* [ ]. For the overlapping transitions $^3H_4 \rightarrow {}^3P_1$ and $^3H_4 \rightarrow {}^1I_6$ a combination of the respective matrix elements has been taken. g_a is the degeneracy of the ground state and is equal to (2J+1). J is the total angular momentum, n is the refractive index, e is the charge of the electron (e =4,803·10^{-10} esu). The factor 10^{36} is necessary to convert calculated intensity from esu^2·cm^2 into Debye^2.

The intensity transitions parameterization is performed in [ ] using the room-temperature absorption spectrum, because of Judd-Ofelt theory requires that all crystal-field levels of the ground state are equally populated. Authors of [ ] was found that parameter Ω_2 is positive, but Ω_4 is larger than Ω_6. It is interesting to note that the situation when $\Omega_4 > \Omega_6$ is also often found for the PbO-PbF_2 glasses [ ]. Moreover it is important to note also that the intensity of the absorption spectra of ZBLAN:Pr^{3+} shows that Judd-Ofelt theory has in the case of trivalent praseodymium only limited validity for the description the dipole strengths of the intraconfigurational 4f→4f transitions. This is mainly due to the small energy "gap" between states of the ground $4f^{(2)}$ and the excited $4f^{(1)}5d$ configurations. In addition, the Ω_λ parameters may show the considerably spread depending on the number of transitions included in the fit.

§1.5. Magnetooptical properties of the rare-earth paramagnetic glasses

It is well-known that the Judd-Ofelt theory [1] provides an effective quantitative description of the parity-forbidden intra-configurational $4f \rightarrow 4f$ transitions observed both in the visible and near ultraviolet spectrum ranges in various rare-earth (RE) compounds. The parity prohibition is removed from such transitions at the expense of odd (static or dynamic [1]) crystal field admixture by the neighboring ($n\ell'$) states of different parity belonging to excited ($4f^{n-1}5d$ or $4f^{n-1}5g$) ion configurations mixed with states of the ground $4f^n$ RE-ion configuration.

A similar mechanism of $4f \rightarrow 4f$ transition "permission" seems to play an essential role in the magnetooptics of RE compounds, as well. For instance, in Refs. [67,68,69], a theoretical scheme similar to that of the Judd-Ofelt theory [19,20] was used to interpret the magnetooptical spectra caused by the forbidden $4f \rightarrow 4f$ transitions. This scheme contains several phenomenological parameters F_λ (usually there are three, i.e., $\lambda = 2, 4, 6$, but in some cases there may be fewer) depending on the asymmetrical field of the RE ion environment in the crystal. These parameters can be determined from the magnetooptical experiment itself, and are common for all electronic transitions within the RE ion $4f^n$ configuration.

Let us now consider the theoretical scheme for interpretation of the magnetooptical spectra [62-64] that is caused by the parity-forbidden intra-configurational $4f \rightarrow 4f$ transitions in more detail, and apply this scheme to the specific case of the magnetooptics of RE paramagnetic glasses.

Magnetic circular dichroism (MCD) is the differential absorption of left-circularly polarized (*LCP*) and right-circularly polarized (*RCP*) light. It is caused by induced optical activity by an external longitudinal magnetic field, where the magnetic field lines are parallel to the propagation direction of the light beam. The MCD formalism has been worked out by Stephens [70] and extended by Piepho and Schatz [71] (see §3.5). Application of the MCD theory on rare-earth ions in crystals and paramagnetic glasses can be found by Görller-Walrand *et al.* [72,73], Collocott *et al.* [74], and Edelman *et. al.* [75]. As shown by Stephens [70], the general expression for MCD is,

$$\Delta\alpha = (\alpha_+ - \alpha_-) = \gamma\mu_B H\left[\frac{A}{\hbar}\cdot\frac{df}{d\omega} + \left(B + \frac{C}{kT}\right)f\right] \qquad (1.45)$$

where H is the magnetic field strength (in gauss), $f = f(\nu, \nu_0)$ is the function of the absorption band contour, ω is the light frequency (in s^{-1}), γ is a constant [70], k is the Boltzmann constant, μ_B is the Bohr magneton, and α_+ and α_- are the absorption coefficients for clockwise and counter-clockwise circularly polarized light radiation, respectively.

A, B and *C* are the Faraday parameters (or MCD parameters [70]). The occurrence of an *A*-term indicates that there is a degeneracy of either the ground state or excited state levels. The *C*-term gives evidence of degenerate ground state levels and reflects a population difference between the Zeeman levels from which the left- and right-circularly polarized light is absorbed. The *B*-term appears when there is a magnetic-field induced mixing of the levels involved, but it is only important in the absence of *A*- and *C*-terms, i.e., when there are no degenerate crystal-field levels.

The *A*- and *C*-members of the MCD or Faraday effect (FE) characterize the contributions to the MCD (or FE) of the magnetooptically-active transitions of a type "singlet → doublet" and "doublet → singlet", respectively, and can be expressed in the general case by the matrix elements of these transitions [70],

$$C = C_{(-)} - C_{(+)} = \frac{1}{d_0}\sum_{a,b}[|<a|\hat{D}^{(1)}_{-1}|b>|^2 - |<a|\hat{D}^{(1)}_{+1}|b>|^2]\cdot<a|\hat{\mu}_Z|a> \qquad (1.46)$$

$$A = A_{(-)} - A_{(+)} = \frac{1}{d_0}\sum_{a,b}[|<a|\hat{D}^{(1)}_{-1}|b>|^2 - |<a|\hat{D}^{(1)}_{+1}|b>|^2]\cdot\left(<a|\hat{\mu}_Z|a> - <b|\hat{\mu}_Z|b>\right), \qquad (1.47)$$

where $\hat{\mu}_z = \frac{1}{2}g_\parallel = g_0 <a|\hat{J}_Z|a>$ is the operator of the *z*-projection of the doublet state magnetic moment (expressed in Bohr magnetons μ_B); d_0 is the degeneracy order of the ground state $|a>$; $g_\parallel \equiv g_z$ is the *z*-component of the *g*-tensor of the doublet ($z||H$); $\hat{D}_{\pm1}$ are components of the dipole moment operator; and $|a>$ and $|b>$ are the wavefunctions of the Stark sublevels of the initial and final states of the magnetooptical transition, respectively.

Substituting the expression for the matrix element of $4f \rightarrow 4f$ transition from eqn. (1.26) into the formula (1.46), let us rewrite it in more convenient form for the further calculations, using the following notations: $L \Rightarrow L_0, S \Rightarrow S_0, J \Rightarrow J_0$ and $L' \Rightarrow L, J' \Rightarrow J, S' \Rightarrow S_0$.

Then we find that[2],

$$B_{tp}B_{t'p'}\begin{pmatrix}1 & \lambda' & t\\ 1 & -(p+1) & p\end{pmatrix}\cdot\begin{pmatrix}1 & \lambda & t'\\ -1 & (p+1) & -p\end{pmatrix} = -\frac{g_0 < J_0 \| \hat{J} \| J_0 >}{(2J_0+1)}\sum_{\lambda\lambda',p}\begin{pmatrix}\lambda & \lambda' & 1\\ -(p+1) & (p+1) & 0\end{pmatrix}\cdot$$
$$(2\lambda+1)(2\lambda'+1)\begin{Bmatrix}\lambda & \lambda' & 1\\ J_0 & J_0 & J\end{Bmatrix}(-1)^{(J_0+J)}\Gamma^{(\lambda)}\Gamma^{(\lambda')}\cdot\sum_{tt'}\begin{pmatrix}1 & \lambda' & t\\ 1 & -(p+1) & p\end{pmatrix}\begin{pmatrix}1 & \lambda & t'\\ -1 & (p+1) & -p\end{pmatrix}B_{tp}B_{t'p'}\cdot \quad (1.48)$$
$$\Xi(t\lambda)\Xi(t'\lambda') = -\frac{g_0 < J_0 \| \hat{J} \| J_0 >}{(2J_0+1)}\sum_{t,p,\lambda}(-1)^{(J_0+J)}\Xi(t\lambda)^2\cdot B_{tp}^2(2\lambda+1)^2\begin{pmatrix}\lambda & \lambda & 1\\ -(p+1) & (p+1) & 0\end{pmatrix}$$
$$\begin{Bmatrix}\lambda & \lambda & 1\\ J_0 & J_0 & J\end{Bmatrix}\begin{pmatrix}1 & \lambda & t\\ 1 & -(p+1) & p\end{pmatrix}^2 |< L_0S_0J_0 \| U^{(\lambda)} \| LSJ >|^2$$

Here we used the following condition: $\Delta M = M - M_0 = (p+1)$, and:

$$C_{(+)} = \frac{1}{d_0}\sum_{MM_0}|< L_0S_0J_0M_0 \,|\, \hat{D}^{(1)}_{+1} \,|\, LS_0JM >|^2 < J_0M_0 \,|\, \hat{\mu}_Z \,|\, J_0M_0 >= \frac{1}{(2J_0+1)}\sum_{MM_0}< J_0M_0 \,|\, \hat{\mu}_Z \,|\, J_0M_0 >\cdot$$
$$\cdot < L_0S_0J_0M_0 \,|\, \hat{D}^{(1)}_{+1} \,|\, LS_0JM >< LS_0JM \,|\, \hat{D}^{(1)}_{-1} \,|\, L_0S_0J_0M_0 >= -\frac{g_0 < J_0 \| \hat{J} \| J_0 >}{(2J_0+1)}\sum_{\lambda\lambda',tt'}(2\lambda+1)(2\lambda'+1)\Xi(t\lambda)\Xi(t'\lambda')$$
$$(-1)^{J_0+J}\cdot\Gamma^{(\lambda)}\Gamma^{(\lambda')}\sum_{pp',MM_0}(-1)^{2J_0+J-M_0-M'_0-M}\cdot(2\lambda+1)(2\lambda'+1)\begin{pmatrix}J_0 & J_0 & 1\\ -M_0 & M'_0 & 1\end{pmatrix}\begin{pmatrix}\lambda' & J_0 & J\\ (p+1) & -M'_0 & M\end{pmatrix}$$
$$\begin{pmatrix}J_0 & \lambda' & J\\ M_0 & -(p+1) & -M\end{pmatrix}B_{tp}B_{t'p'}\cdot\begin{pmatrix}1 & \lambda & t\\ 1 & -(p+1) & p\end{pmatrix}\begin{pmatrix}1 & \lambda' & t'\\ -1 & (p+1) & -p\end{pmatrix} = \frac{g_0 < J_0 \| \hat{J} \| J_0 >}{(2J_0+1)}\sum_{t,p,\lambda}(-1)^{(J_0+J)}\Xi(t\lambda)^2$$
$$B_{tp}^2(2\lambda+1)^2\begin{pmatrix}\lambda & \lambda & 1\\ -(p+1) & (p+1) & 0\end{pmatrix}\cdot\begin{Bmatrix}\lambda & \lambda & 1\\ J_0 & J_0 & J\end{Bmatrix}\begin{pmatrix}1 & \lambda & t\\ 1 & -(p+1) & p\end{pmatrix}^2 |< L_0S_0J_0 \| U^{(\lambda)} \| LSJ >|^2$$

(1.49)

where g_0 is the Lande' factor of the ground multiplet and $< J_0 \| \hat{J} \| J_0 >= \sqrt{J_0(J_0+1)(2J_0+1)}$ is the doubly reduced matrix element of angular momentum [76]; in (2.34) has been used that: $\Delta M = M - M_0 = -(p+1)$.

For the fixed values of q and M, M_0 we have in (1.48) and (1.49) an obvious equality: $p = p'$, which follows from the well-known properties of 3j-symbols [47],

[2] Doubly reduced matrix elements $< f^n\phi J \| U^{(\lambda)} \| f^n\phi' J' >$ satisfy to the following relation [47]:
$< f^n\phi J \| U^{(\lambda)} \| f^n\phi' J' >= (-1)^{J-J'} < f^n\phi' J' \| U^{(\lambda)} \| f^n\phi J >^*$

i.e., the 3*j*-symbol equals zero unless the sum of the projections is equal to (m_1 + m_2 + m_3) = 0. Note that the summation of the eqns. (1.48) and (1.49) over the momentum projections M and M_0, was obtained by using the following identity [47],

$$\sum_{\mu_1\mu_2\mu_3}(-1)^{l_1+l_2+l_3+\mu_1+\mu_2+\mu_3}\begin{pmatrix} j_1 & l_2 & l_3 \\ m_1 & \mu_2 & -\mu_3 \end{pmatrix}\begin{pmatrix} l_1 & j_2 & l_3 \\ -\mu_1 & m_2 & \mu_3 \end{pmatrix}\begin{pmatrix} l_1 & l_2 & j_3 \\ \mu_1 & -\mu_2 & m_3 \end{pmatrix}=\begin{pmatrix} j_1 & j_2 & j_3 \\ m_1 & m_2 & m_3 \end{pmatrix}\begin{Bmatrix} j_1 & j_2 & j_3 \\ l_1 & l_2 & l_3 \end{Bmatrix} \tag{1.50}$$

By using the relation given in (1.50) in eqns. (1.48) and (1.49), we can apply the following replacements: $\mu_1 = -M_0'$, $\mu_2 = -M_0$, $\mu_3 = -M$, m_1 = − (p+1) (or (p+1) in (1.50)), m_2 = (p+1) (or −(p+1) in (1.50)), m_3 = 0, $j_1 = \lambda$, $j_2 = \lambda'$, $j_3 = 1$, and $l_1 = J_0$, $l_2 = J_0$, $l_3 = J$. It is important to note that in the summation in the eqns. (1.48) and (1.49) over the momentum projections M, M_0, we have added the formal summation over the momentum projection M_0', that does not change the final result. Therefore, substituting (1.48) and (1.49) into the formula (1.46), we find that eqn. (1.46) can be rewritten in the following compact form [67-69],

$$C = \frac{1}{(2J_0+1)}\sum_{\lambda} F_\lambda \cdot (-1)^{J_0+J}\begin{Bmatrix} \lambda & \lambda & 1 \\ J_0 & J_0 & J \end{Bmatrix}\cdot g_0 < J_0 \| \hat{J} \| J_0 > \cdot |< L_0 S_0 J_0 \| U^{(\lambda)} \| LSJ >|^2, \tag{1.51}$$

where parameters F_λ are equal to,

$$F_\lambda = 2\sum_p \begin{pmatrix} \lambda & \lambda & 1 \\ (p+1) & -(p+1) & 1 \end{pmatrix} |\varphi^{(\lambda)}_{p,+1}|^2 \tag{1.52}$$

and $|\varphi^{(\lambda)}_{p,+1}|^2 = \sum_t (2\lambda+1)^2 \cdot B^2_{tp}\, \Xi^2(t\lambda)\begin{pmatrix} 1 & \lambda & t \\ 1 & -(p+1) & p \end{pmatrix}^2$. Note that an obvious equality, $\lambda' = \lambda$, used in eqns. (1.48), (1.49) and (1.46) follows from a consideration of the triangle condition $\Delta(\lambda, \lambda', 1)$ for the 3*j*- and 6*j*-symbols in eqns. (1.48) and (1.49). In addition, the equality, $t' = t$, can be obtained by a simultaneous carrying out of the relation $\lambda' = \lambda$ and the triangle condition $\Delta(\lambda, t, 1)$ for the 3*j*-symbols in eqns. (1.48) and (1.49), for which t = ($\lambda \pm 1$).

Valiev et al. [68,69] have shown that the Judd-Ofelt mechanism of removing the forbidden character from intra-configurational $4f \rightarrow 4f$ transitions plays an important role in the magnetooptics of disordered RE-compounds (solutions and

paramagnetic glasses). According to their investigation, the main factor determining the features of an energy spectrum and wavefunctions of the RE-ions in disordered media are the fluctuations of the local parameters of both the even and odd crystal field. Indeed, supposing that the CF-parameter fluctuations are independent, and that they carry the statistical average of the odd CF coefficient combinations $A_{tp}*A_{t'p'}$ (which are included in eqn. (1.52) for the F_λ parameters) over all possible orientations of RE centers in disordered media, we can obtain the following useful expression [69],

$$F_\lambda = \sqrt{\frac{2}{3}}\sum_t (2\lambda+1)\begin{Bmatrix}\lambda & 1 & t\\ 1 & \lambda & 1\end{Bmatrix}\Omega_\lambda(t)\ , \qquad (1.53)$$

where $\Omega_\lambda(t)$ is the partial contribution to the Judd-Ofelt parameter Ω_λ due to a specific value of *t*, i.e., $\Omega_\lambda = \sum_t \Omega_\lambda(t)$.

We can characterize the magnetooptical activity (MOA) of a single electron transition by the magnitude (and sign) of the ratio of the paramagnetic *C*-term (2.36) to the *D*-term, the dipole strength (or "line strength" *S* from eqn. (1.22)) of the transition. In this case, the expression for *C*/*D* is proportional in general to the magnetic moment of the RE ion ground state in the crystal [70]. Consequently, it is easy to determine the *C/D* ratio from the numerical integration of the temperature dependence of the MCD and the optical absorption bands, accordingly to method of moments [70]. On the other hand, by using eqns. (1.51), (1.53) and (1.22), we find the ratio of the partial contributions to *C* and *D* for the $S_0L_0J_0 \rightarrow SLJ$ transition can be represented as,

$$\frac{C(t,\lambda)}{D(t,\lambda)} = (-1)^{J_0+J}\sqrt{\frac{3}{2}}\cdot g_0\mu_B < J_0 \| \hat{J} \| J_0 > (2\lambda+1)\begin{Bmatrix}\lambda & \lambda & 1\\ 1 & 1 & t\end{Bmatrix}\begin{Bmatrix}\lambda & J_0 & J\\ J_0 & \lambda & 1\end{Bmatrix} = \frac{g_0\mu_B}{8\lambda(\lambda+1)}\left[t(t+1)-\lambda(\lambda+1)-2\right]\cdot \qquad (1.54)$$
$$\cdot\left[J(J+1)-J_0(J_0+1)-\lambda(\lambda+1)\right]$$

This simple analysis shows that the tolerable limiting *C/D* factor is,

$$\left|\frac{C}{D}\right| \le \frac{1}{2}g_0(J+1)\mu_B \quad . \qquad (1.55)$$

As the index *t* has two values $t = \lambda \pm 1$ at fixed λ, we can obtain from (1.54),

$$\frac{C(\lambda-1,\lambda)}{D(\lambda-1,\lambda)} = -\frac{(\lambda+1)}{\lambda}\cdot\frac{C(\lambda+1,\lambda)}{D(\lambda+1,\lambda)}\ , \qquad (1.55)$$

so that the corresponding ratios always have different signs. By taking into account that $D(t,\lambda) \geq 0$, it is possible to conclude that the terms in C with different t always compensate each other, given a specific λ. If any term of the odd CF (with definite index t) plays an essential role in the mechanism to remove the forbidden character of the $4f \rightarrow 4f$ transition, the *C/D* ratio may be written as follows,

$$\frac{C(t)}{D(t)} = \frac{\sum_{\lambda}\frac{g_0\mu_B}{8\lambda(\lambda+1)}\left[t(t+1)-\lambda(\lambda+1)-2\right]\cdot\left[J(J+1)-J_0(J_0+1)-\lambda(\lambda+1)\right]\cdot\Omega_\lambda(t)\cdot|< S_0L_0J_0 \parallel U^{(\lambda)} \parallel LSJ >|^2}{\sum_{\lambda}\Omega_\lambda(t)\cdot|< S_0L_0J_0 \parallel U^{(\lambda)} \parallel LSJ >|^2} \qquad (1.56)$$

where $\Omega_\lambda(t)$ is the partial contribution of the term with a specific t to the Judd-Ofelt parameter Ω_λ.

As a consequence, the corresponding comparison between the experimentally determined value of the *C/D* ratio and the theoretically calculated values of the corresponding partial contribution ratios, yields important information, not only on the application limits of the Judd-Ofelt theory, but also on the role of the different odd CF terms in the mechanism of removal of the forbidden character from $4f \rightarrow 4f$ transition. Indeed, the excellent agreement between the theoretically calculated ratio *C/D* and the experimental data for the paramagnetic phosphate glass $Er(PO_3)_3$ obtained in Ref. [69] testifies to the dominant contribution of admixing between the excited $4f^{n-1}5d$ ($l'=2$) configuration states and the states of the ground $4f^n$ configuration. This assumption considerably rationalizes the results of interpretation of MCD data observed for the $4f \rightarrow 4f$ transitions to excited $^4F_{3/2}$ and $^4F_{5/2}$ multiplets of Er^{3+} in the paramagnetic phosphate glass, $Er(PO_3)_3$.

Thus, we see that the theoretical scheme developed in [67-69] and based on the three-parameter Judd-Ofelt theory [19,20] can be used successfully for the quantitative description of the MCD (and Faraday effect) spectra in RE paramagnetic glasses through the use of the phenomenological parameters F_λ (λ

= 2, 4, 6) determined by experimental methods. In addition, based on these assumptions, it seems reasonable to conclude that the static character of the odd CF terms provides a satisfactory explanation for the removal of the parity prohibition from the $4f \rightarrow 4f$ ED transitions, with the dominant contribution of mixing coming from an excited-state configuration ($4f^{n-1}5d$ or $4f^{n-1}5g$) of the RE ion.

The experimental MCD spectra have been treated using the highly efficient method of moments [39,40], which permits one to connect the observed changes of the integrated parameters of the MCD bands (such as band area, bandwidth, etc.) with the electronic micro parameters of the magnetic ions (magnetic moment of the ground state, etc.). In particular, the temperature of the MCD band zeroth moment $<\theta_0>$ can be related along with the temperature-dependent paramagnetic contribution (*C*-term) to the magnetooptical activity (MOA) by [39,43],

$$< \theta_0 >= -\gamma\left[\frac{C}{kT} + B\right] \quad , \qquad (1.57)$$

where *C* and *B* are the partial contributions of the paramagnetic and mixing terms of the MOA, respectively, and $\gamma = (2\pi^2 N / 3c\bar{n}\hbar)\cdot(\bar{n}^2+2)^2/9$. In the latter equation, *N* is the number of magnetoactive ions (per cm^3) and $\bar{n}$ is the average index of refraction of the medium.

At the same time, the *C*, *B* and *A*-terms of the MOA can be calculated (see also Refs. [39,40]) by using specific models of the energy structure and the wavefunctions of the RE-ion ground and excited states. In addition, the MOA of the electronic transitions can be characterized by the factor *C/D* defined as the ratio of the paramagnetic *C*-term of the MOA to the dipole transition strength *D* proportional to the oscillator strength *f* of the optical transition [39,40,43]. The magnitude of the *C/D* factor is determined by the ground state magnetic moment of the RE-ion, while its sign is related to the symmetry of the electronic transition [39,40]. On the other hand, both the magnitude and sign of the *C/D* factor can be determined by numerical integration of the MCD and the absorption bands at different temperatures [43],

$$2\frac{<\theta_0>}{<\alpha_0>} = -\frac{1}{D}\left[\frac{C}{kT} + B\right] \qquad (1.58)$$

where $<\alpha_0>$ is the zeroth moment of absorption band.

The method of the MCD moments has been applied for the determination of the Faraday parameters: *A*, *B* and *C* of fluorozirconate (ZBLAN) glass doped by Pr^{3+} in [ ] gave reproducible results only for the *B* and *C* parameters, but not for *A*. A linear relation between the zeroth moment of the MCD and 1/T was found for the temperature interval 77 – 300K. For example, the result of the moment analysis for the transition $^3H_4 \rightarrow {}^3P_0$ showed that the value of *C/D* factor is *C/D* = - 0,91μ_B. It is important to note that the theoretical calculation of this ratio *C/D* for given 4*f* → 4*f* transition executed with use of equation (1.56) at λ = 4, *t* = 5, J_0 = 4 and *J* = 0 shows that *C/D* = - 1,6 μ_B, i.e. found value of *C/D* ratio is in satisfactory agreement with an experimental estimation. At the same time, *B*/*D* ratio is small for all observed transitions.

Chapter 2. EXPERIMENTAL DEVICES. SAMPLES

§2.1. Paramagnetic glasses samples and their preparation

The precursor glasses and glass ceramics doped with Er^{3+}/Yb^{3+} were prepared with the following compositions (in mol%): $30SiO_2(16\text{-}x)AI_2O_340PbF_210CdF_2$ $xEr_2O_34Yb_2O_3$ (x = 0.5, 1.0, 2.0, 4.0) [36][3]. For each batch, starting materials of about 20 g were fully mixed and melted in a covered platinum crucible in air at 1000 °c for 2 h, and then cast onto a steel plate. The precursor glasses obtained were then annealed for 8 h at the glass transitions temperature to induce crystallizations.

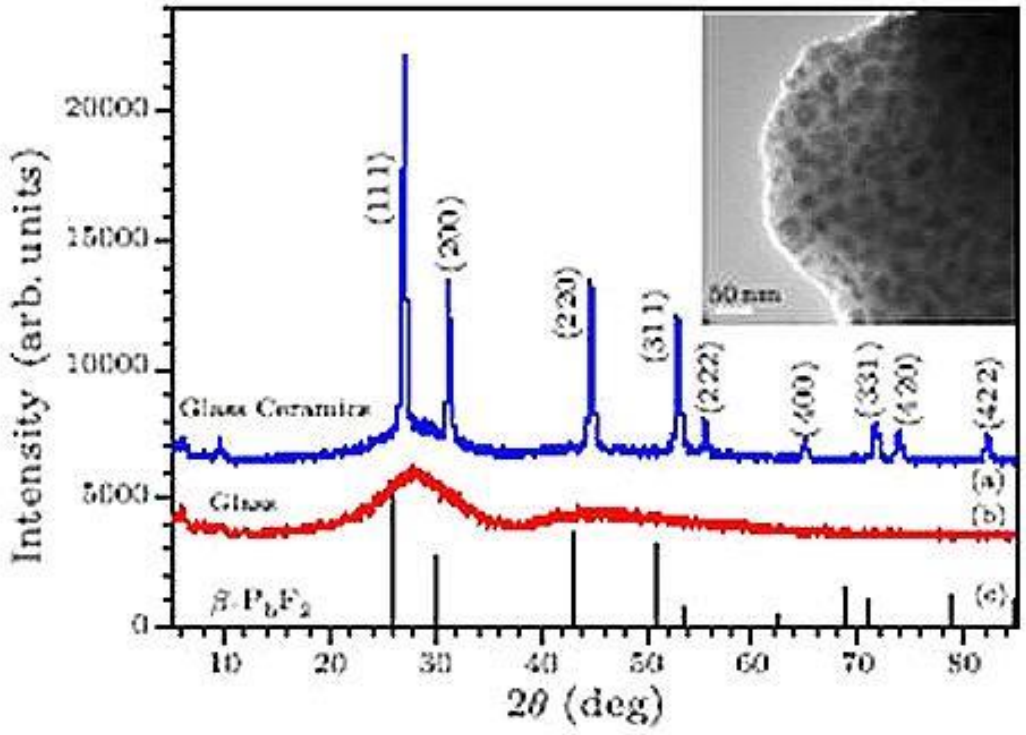

Fig. 2. XRD patterns of (*a*) the oxyfluoride glass, (*b*) the oxyfluoride glass ceramic and (*c*) standard β-PbF_2 crystals [36]. Inset: TEM image of oxyfluoride glass ceramic.

The X-ray diffraction (XRD) patterns of the precursor glass and treated glass were recorded, as shown in Figs. 2(a) and 2(b). Figure 2(c) is the standard XRD of β-PbF_2 crystals. Compared with the standard β-PbF_2 crystals, the diffractive peaks of the glass ceramics doped with Er^{3+}/Yb^{3+} in Fig. 2(b) are clearly shifted. This implies

[3] The samples of the paramagnetic rare-earth glasses were prepared in Novel Fluorescent Materials and Devices Laboratory at APS, TEDA, Nankai University (China).

that the nanocrystals are a mixture of β-PbF_2 and fluoride of rare-earths Er^{3+}/Yb^{3+} ions were doped into fluoride nanocrystals. The size of fluoride nanocrystal is about 20nm according to the Sheerer formula. The inset in Fig.2 is an image from the transmission electron microscopy (TEM). It shows that the fluoride nanocrystal doped with Er^{3+}/Yb^{3+} was dispersed well in the host matrix. The oxyfluoride glass after thermal treatment, with fluoride nanocrystal doped with Er^{3+}/Yb^{3+}, was called oxyfluoride glass ceramic doped with Er^{3+}/Yb^{3+} [36].

An oxyfluoride glass samples containing a small concentration of the fluoride nanocrystal doped by Er^{3+}/Yb^{3+} clusters have been cut in the form of thin plates of thickness ~ 1mm. After that these thin plates have polished with using of diamond pastes with slowly thinning grain (up to ~1 μm) for the performing of optical and magnetooptical studies.

§2.2. Experimental device for the measuring of an optical absorption

The absorption spectra in non-polarized light of the oxyfluoride glass samples doped by Er^{3+}/Yb^{3+} ions were recorded in the region of the some absorption bands of the Er^{3+} ion at 85K and 300K on a modified single-beam spectrophotometer, which was made on the base of a double diffraction monochromator MDR-23[4]. The absorption spectra (to be specific, the spectra of optical density *D)* were recorded with a spectral resolution of 2-3 cm^{-1} (or better) using the technique of stabilization of the average photomultiplier (PMT) current. In this case, one records in the course of scanning the spectrum under study a signal that is proportional to the high voltage applied to photomultiplier dynodes. Due to the feedback, which encloses a photomultiplier and a HV source, and a nonlinear current-voltage characteristic of the PMT used in the measurements (PhM - 71, 100), the change of dynode voltage ΔU_D, corresponds

[4] The absorption spectrum of the oxyfluoride glass samples doped by Er^{3+}/Yb^{3+} ions in the visible and near-infrared spectral region at T = 300K was recorded on the spectrophotometer "Hitachi U – 4100" in Novel Fluorescent Materials and Devices Laboratory at APS, TEDA, Nankai University (China).

to the relative change of the PMT photocathode illumination $\frac{\Delta\Phi}{\Phi}$, which is caused by light absorption in the crystal, and we have [37]:

$$\Delta U_D = K \cdot \frac{\Delta\Phi}{\Phi} = K \cdot D \qquad (2.1)$$

where Φ is the light flux and K is the scale factor.

To cool the sample, it was placed in a liquid nitrogen bath of an optical cryostat between two quartz bars (~ 50 mm) having the polished surfaces on the ends of bars. The polished external ends of the quartz bars are heated by means of the wire stoves to avoid their freezing in the measuring process.

§2.3. Experimental devices for the measuring of the magnetic circular dichroism and magnetic circular polarization of luminescence

MCPL The MCPL (and luminescence) spectra of the oxyfluoride glass samples doped by Er^{3+}/Yb^{3+} ions were studied in the vicinity of the radiative transition $^4F_{9/2} \rightarrow {}^4I_{15/2}$ (the "red" band of the fluorescence) with spectral resolution ~ 5-10 cm^{-1} near 15400 cm^{-1} in the temperature range 90 - 300 K using a highly sensitive measurement apparatus performed on the base of the double diffraction monochromator MDR-23. Both the excitation and observation of the luminescence were done in “transmission” geometry for longitudinal (relative to light propagation) magnetization in the external field H (up to 10 kOe). Non-polarized photoexcitation was produced by a mercury lamp (250W) with a UV filter UVB - 5.

The degree of circularity of the luminescence, $P = \frac{I_+ - I_-}{I_+ + I_-}$, where $I_\pm$ are the intensities of the right- and left-circularly polarized components of the luminescence) was measured using a (phase-) controlled "circular analyzer [38], which was a photoelastic modulator of the light radiation with optical feedback [39] and was located in front of the exit linear polarizer, and its plane of the transmission was oriented at an angle of 45° relative to the induced axes of the active element of the modulator. The MCPL spectra were recorded using a PhM -

71 photomultiplier whose dc photocurrent was stabilized to within ~ 2-3 %. The ac component of the photocurrent, which is proportional to *P* (in relative units), was amplified, synchronously detected, and recorded with using of PC. The error in determining the degree of MCPL was ~ 3-5 % in the central region of the luminescence band and increased to ~ 7-10 % at the band edges. The temperature of the sample, which was located in an optical cryostat, varied by no more than 1K.

MCD In the magnetooptical experiments (MCD, FE) on a through-passing light was used a high-aperture geometry of experiment in which natural (i.e. completely nonpolarized) light radiation is projected onto the sample under study placed in an external magnetic field *H*. In this case the MCD degree due to the difference in the absorption coefficients α_+ and α_- for clockwise- and counterclockwise-polarized radiation (per length unity) was defined by measuring the frequency dependencies of the circularity degree *P* of partially polarized light appearing while passing through the magnetized sample the natural light: $P = \frac{1}{2}(\alpha_+ - \alpha_-)$ [37]. These studies were carried on with the experimental installation completely identical to that used to measure the MCPL degree spectra with a Xe-lamp instead of a mercury one being a continuum spectrum source.

MCD spectra were recorded at different temperatures between 85 K (liquid nitrogen) and room temperature on a magnetic circular dichroism spectrophotometer performed on the base of diffraction monochromator MDR-23 extended with an electromagnet. The optical design of this instrument coincides with the design of conventional MCD spectropolarimeter [38]. Light radiation from a water-cooled high intensity 200 W xenon arc falls through fused silica lens on the sample is placed in the pole gap of an electromagnet. The gap is large enough to contain the sample compartment of the optical dewar. In the poles, a hole is drilled for the light beam. The magnetic field strength is approximately 10000 Oe (1,0 Tesla). If the magnetic field is switched off, the instrument can be used to measure of circular dichroism (CD). After sample the light beam is focused on the

entrance slit of double diffraction monochromator MDR-23. The wavelength mechanism of MDR-23 operates from 200 to 850 nm. The wavelength accuracy is 0,1 nm from 200 to 850 nm. The wavelength resolution is ± 0.05 nm at 500 nm.

The dispersed light radiation from the exit slit of the monochromator passes through a special achromat lens into a photoelastic modulator, which converts the linearly polarized light to left- and right-circularly polarized light. The light beam is alternating between left- and right-circular polarization. After the modulator, the modulated light beam passing a linear polarizer is focused by a fused silica lens on the cathode of a photomultiplier tube whose dc photocurrent was stabilized to within ~ 2-3 %. The ac component of the photocurrent, which is proportional to the degree of partially polarized light, P (in relative units), is amplified, synchronously detected, and after corresponding processing of the experimental data with using of the special software ("Origin 6,1" and etc.) on a PC these data are recording in the PC memory. The sensitivity of this instrument is better than 0.5 millidegrees, which corresponds to $1{,}5 \cdot 10^{-5}$ absorbance units. A spectral band width of 0.1 to 0.2 nm was used. The sample can be cooled in an optical cryostat, which operates in the temperature range from 85 K to room temperature and which can be used for both absorption and MCD (or MCPL) measurements.

Chapter 3. EXPERIMENTAL DATA AND DISCUSSION

§3.1. Optical absorption experimental data.

Absorption spectra of the oxyfluoride glass ceramic doped with Er^{3+}/Yb^{3+} ions were measured between 350 and 1600 nm, representing transitions from the ground-state multiplet manifold $^4I_{15/2}$ to the high-energy manifolds $^4I_{13/2}$, $^4I_{9/2}$, $^4I_{5/2}$, $^2H_{11/2}$, and $^4G_{11/2}$ of Er^{3+} ions ground $4f^{11}$-configuration (see Fig. 1). Absorption spectra of Yb^{3+} ions were also obtained between 900 and 1050 nm, representing transition from ground multiplet manifold $^2F_{7/2}$ to the high-energy $^2F_{5/2}$ manifold. belonging to the Yb^{3+} ions ground $4f^{13}$-configuration. Spectra were recorded at

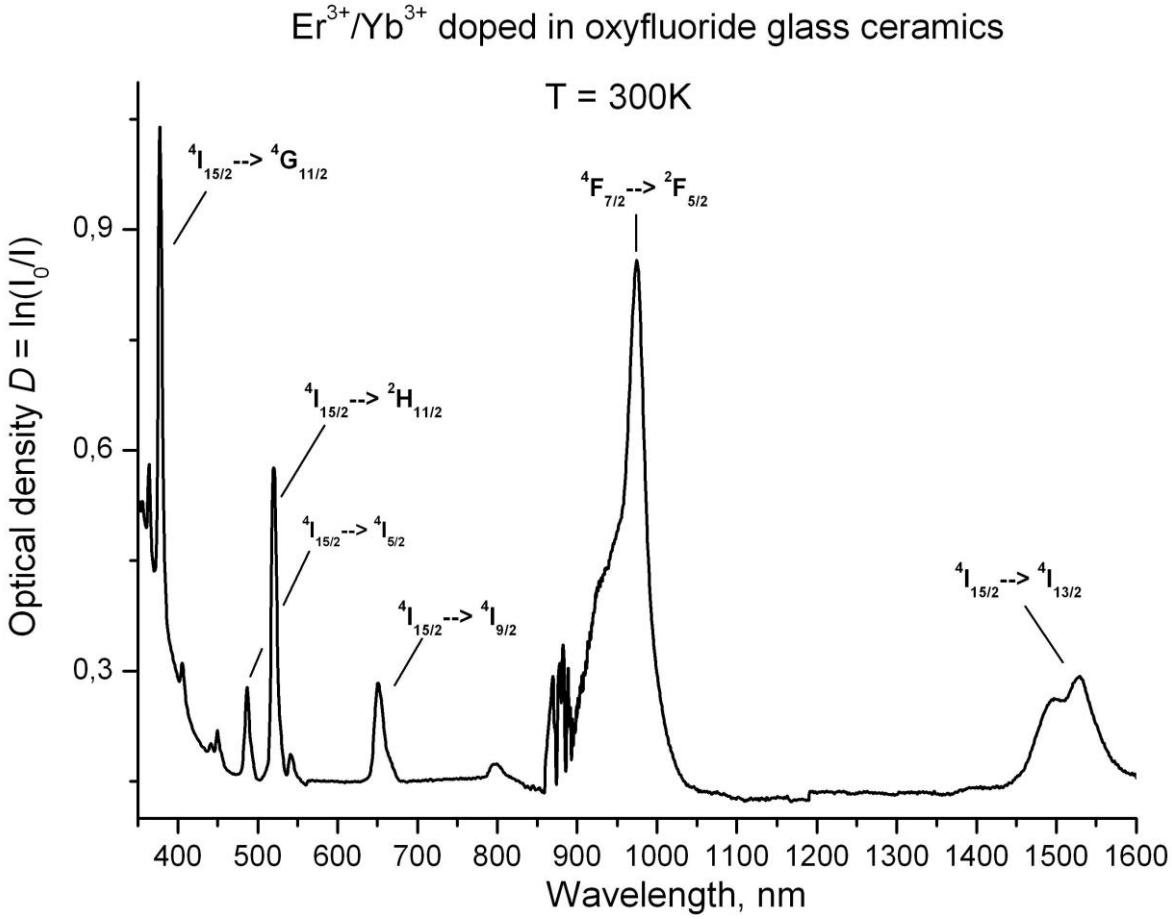

Fig. 1. Optical absorption spectrum of oxyfluoride glass ceramic doped with Er^{3+}/Yb^{3+} ions measured at T = 300 K.

sample temperature 300 K with using of the spectrophotometer "Hitachi U-4100" controlled by a desktop computer and located in Novel Fluorescent Materials and Devices Laboratory at APS, TEDA, Nankai University (China).

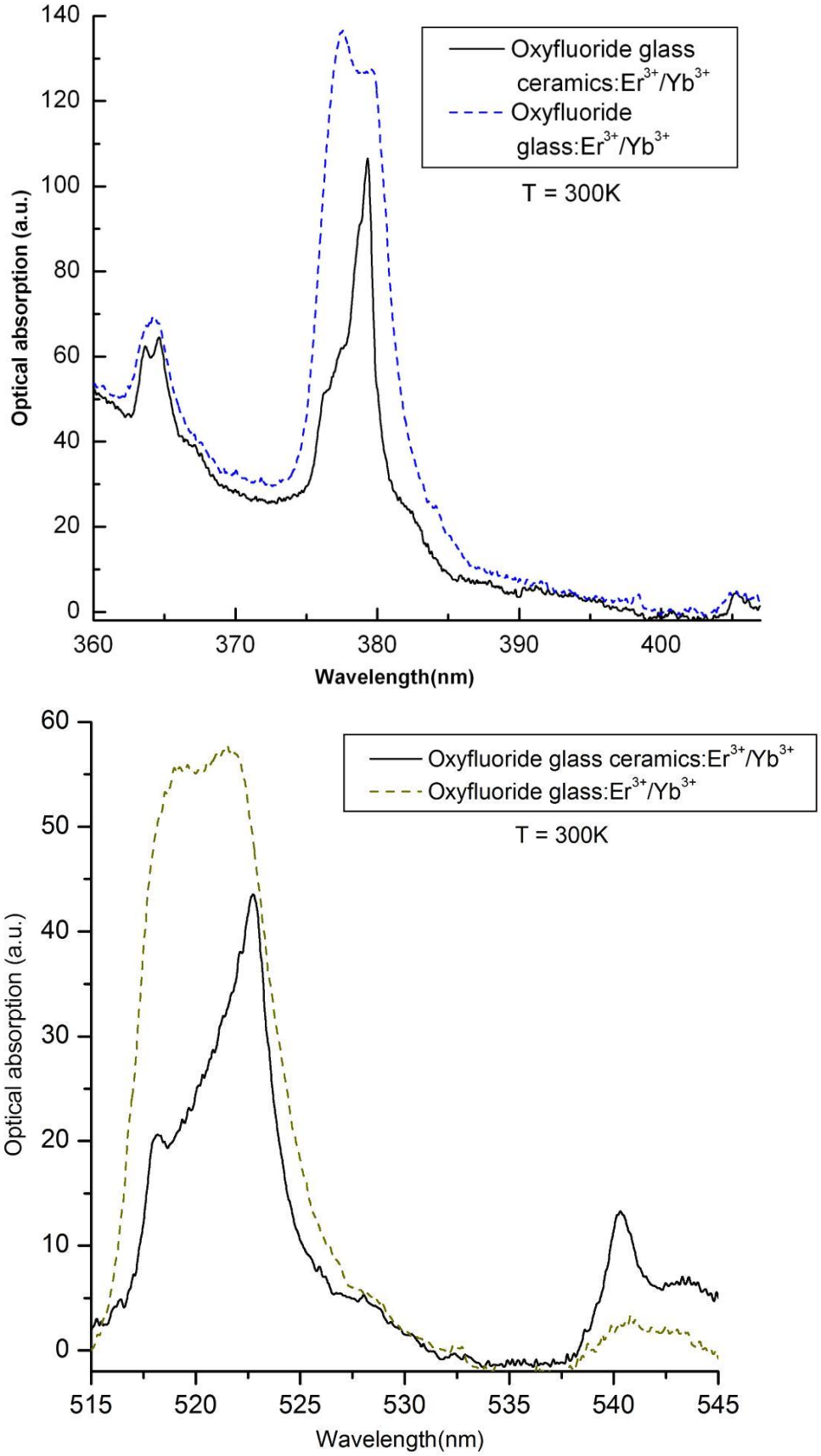

Fig. 2. Optical absorption spectrum of the doped by Er^{3+}/Yb^{3+} ions the ordinary oxyfluoride glass and oxyfluoride glass ceramic measured at T = 300 K in the different spectral regions.

Spectra were recorded at 0.1nm wavelength intervals with an average spectral bandwidth of 0.2nm over the wavelength range investigated. Due to instrumental limitations, we were not able to extend the wavelength measurements further into the near ultraviolet (UV) region to observe the absorption spectrum for the optical transitions to the $^4G_{7/2}$, $^2K_{15/2}$, $^2K_{13/2}$ and other high-energy multiplet manifolds.

To probe the unresolved spectra of the doped by Er^{3+}/Yb^{3+} ions ordinary oxyfluoride glass and oxyfluoride glass ceramic obtained from "Hitachi U- 4100" spectrophotometer, we used a high-resolution double diffraction monochromator MDR Model 23 ("LOMO", Russian) located in the magnetooptical laboratory of Faculty of Physics (NUUz). The instrument has a spectral resolution generally better than 0.05 nm over the wavelength range covered from the $^4I_{15/2} \rightarrow {}^4I_{9/2}$ to $^4I_{15/2} \rightarrow {}^4G_{11/2}$ absorption (Fig. 2) and the fluorescence from the $^4I_{9/2}$ to $^4I_{15/2}$

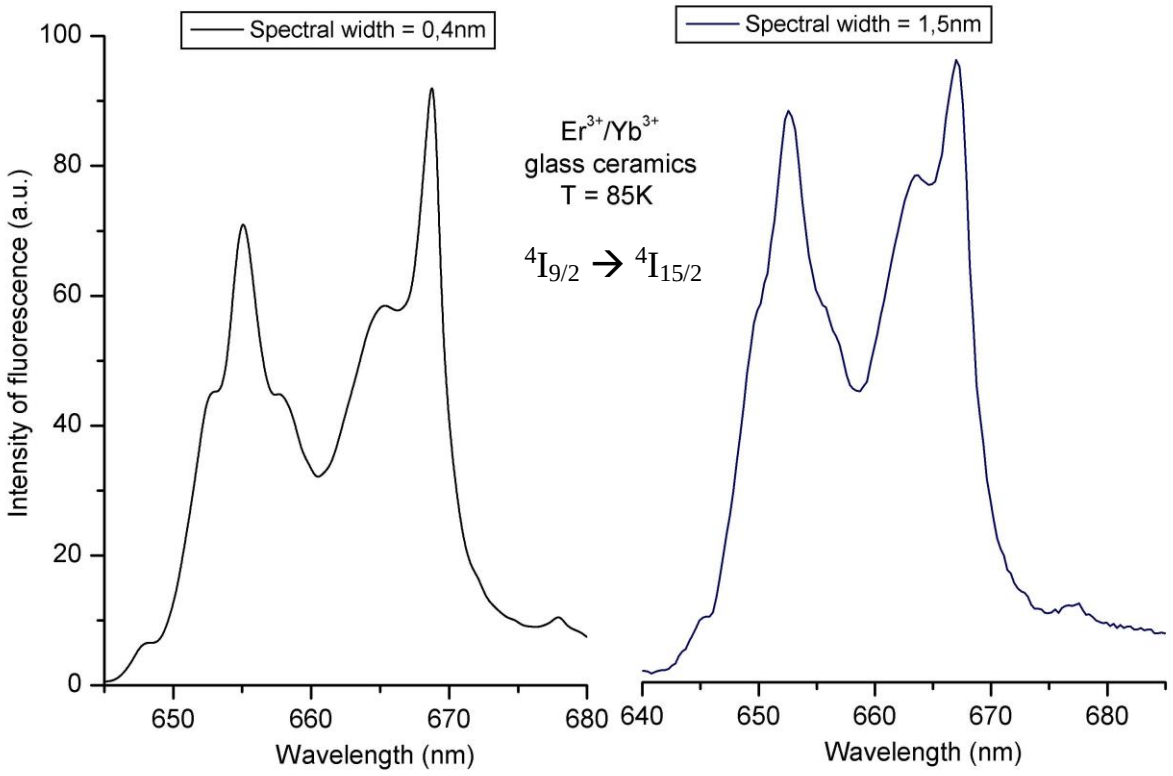

Fig. 3. Measured spectrum of the luminescence $^4I_{9/2} \rightarrow {}^4I_{15/2}$ band in oxyfluoride glass ceramic doped with Er^{3+}/Yb^{3+} ions is shown for the two different optical resolutions at temperature T = 85K.

multiplet manifolds (370 - 680 nm). For these studies, samples were immersed directly into liquid nitrogen (78K) or cooled to 85K in a conduction dewar filled with liquid nitrogen. The absorption spectrum of $^4I_{15/2} \rightarrow {}^2H_{11/2}$, $^4I_{15/2} \rightarrow {}^4I_{7/2}$ and

$^4I_{15/2} \rightarrow {}^4S_{3/2}$ was obtained by placing the oriented sample between two quartz light guides and immersing it into a liquid nitrogen bath. A calibrated photomultiplier tube and a 200W xenon lamp were used for detection and as the excitation source for the absorption spectra, respectively.

For measurements of the fluorescence spectra with using of double diffraction monochromator MDR Model 23, a 250W mercury lamp with assorted UV filter (UVB-5) was used. Note that for the more visibility, the spectrum of luminescence $^4I_{9/2} \rightarrow {}^4I_{15/2}$ band observed in oxyfluoride glass ceramic doped with Er^{3+}/Yb^{3+} ions is shown in Fig. 3 was recorded for the two different optical resolutions at T = 85K.

§3.2. Magnetooptical experimental data and their discussion.

MCD Using of the optical absorption spectra allows us to directly study the multiplet levels of the $4f^n$ and $4f^{n-1}5d$ (or $4f^{n-1}5g$) configurations of the trivalent lanthanide ions observed at higher energies [1-3,17]. But in some cases the MCD spectroscopy, which measures the differential absorption of left- and right-circularly polarized light passing through the sample magnetized by a longitudinal magnetic field *H* can help resolve complicated spectroscopic problems arising in the optical measurements.

The fundamental principles of MCD spectroscopy in detail were described by *Stephens* [40] and *Binnemans et al.* [31]. They noted that the major advantage of MCD spectroscopy compared to absorptive Zeeman spectroscopy is that the individual crystal-field levels, which are not resolvable in the absorption spectra can be successfully distinguished in the MCD spectra in cases where the absorption band width is larger than its Zeeman splitting [31,35,37]. On the other hand, at the simulation of MCD spectra it is possible to determine the symmetry and reliability of the wave functions of the quantum states connected by magnetooptically active absorptive transitions [22,37,40].

MCD spectroscopy uses the numerical integration of the MCD spectral dependence within absorption band for the obtaining of the detailed information regarding the values of the temperature-dependent (~1/*T*) so called “paramagnetic”

(*C*-term), and temperature-independent "diamagnetic" (*A*-term) and "mixing" (*B*-term) contributions to the MCD [31,35,37,40].

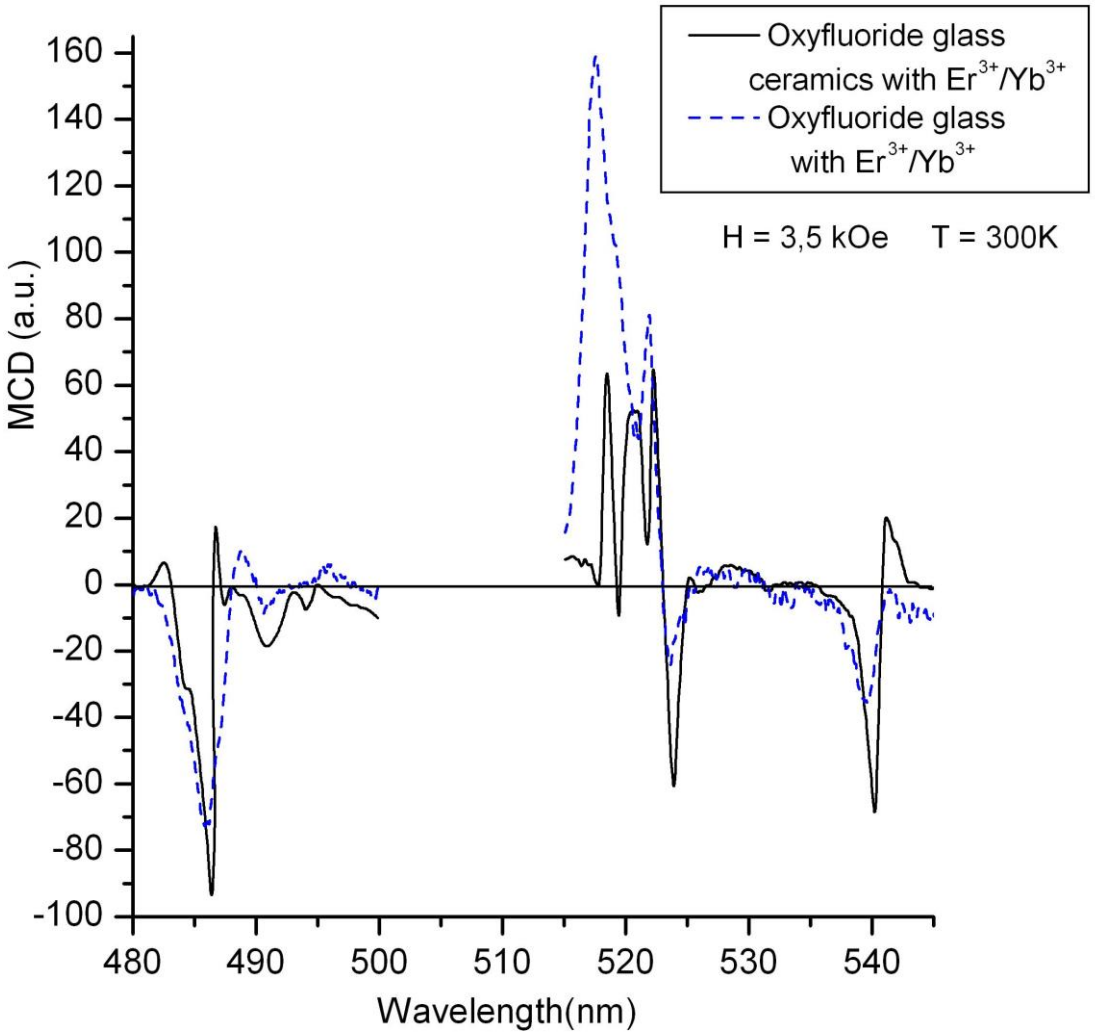

Fig. 4. MCD spectra of the doped by Er^{3+}/Yb^{3+} ions the ordinary oxyfluoride glass and oxyfluoride glass ceramic measured at temperature T = 300 K on the 4f → 4f transitions: $^4I_{15/2} \rightarrow {}^4I_{5/2}$, $^4I_{15/2} \rightarrow {}^2H_{11/2}$ and $^4I_{15/2} \rightarrow {}^4S_{3/2}$ bands.

The MCD spectrum is a superposition of three terms: an *A*-term with the shape of the first derivative of an absorption band, and a *B*-term, and a *C*-term with the shape of an absorption band. MCD signal have a sign. According to the conventional notations [31,35], an *A*-term is positive if the left circularly polarizes light is absorbed to the Zeeman component at high energy. This corresponds to a positive lobe at the high wavenumber side of the MCD spectrum. Both a *B*-term, and a *C*-term are positive if the corresponding MCD signal shows a positive sign.

Thus the MCD of the doped by Er^{3+}/Yb^{3+} ions ordinary oxyfluoride glass and oxyfluoride glass ceramic measured at T 300 K (Fig. 4) shows a positive *A*-term

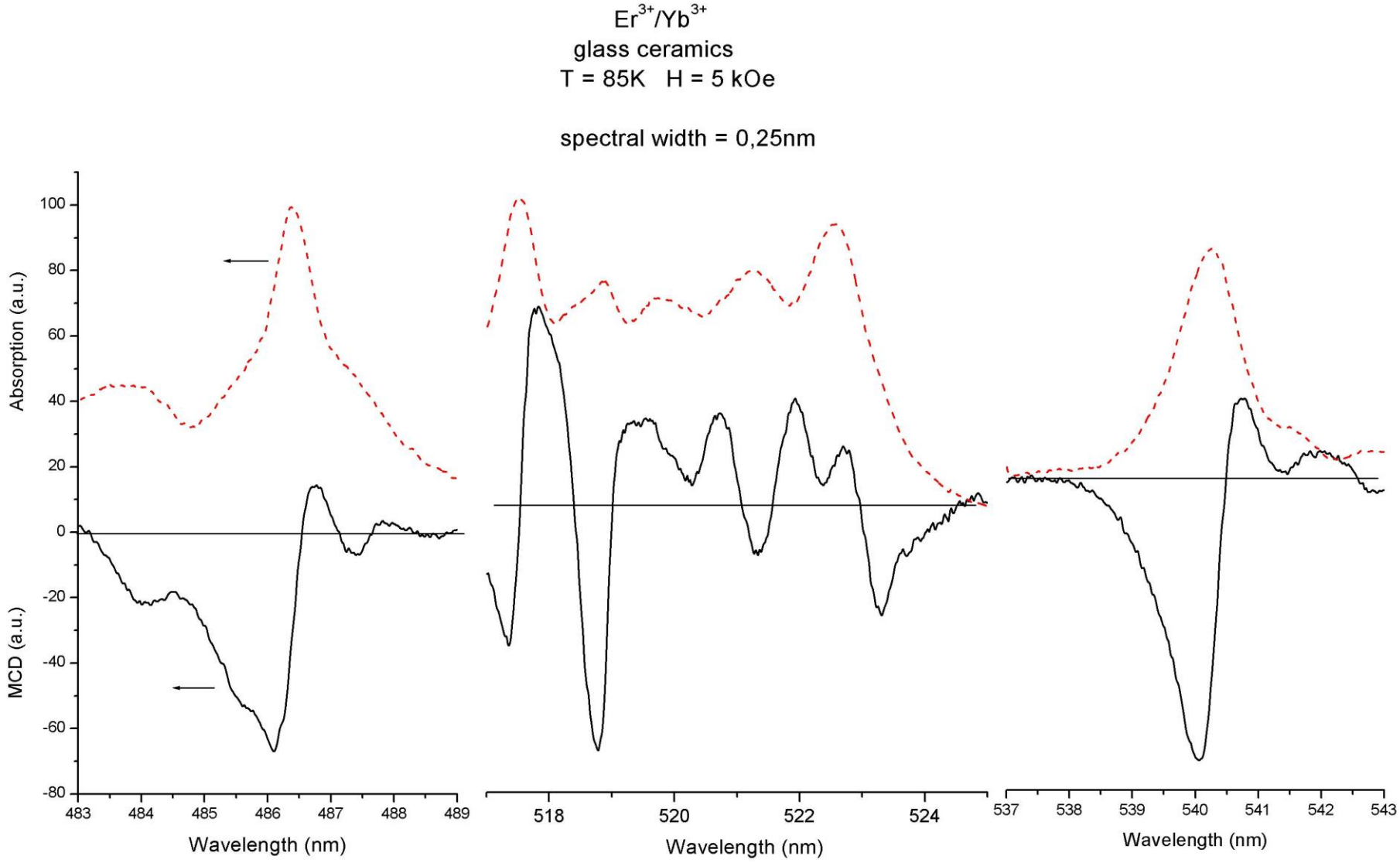

Fig. 5. MCD spectra of the oxyfluoride glass ceramic doped by Er^{3+}/Yb^{3+} ions measured at temperature T = 85 K on the 4f → 4f transitions: $^4I_{15/2}$→ $^4I_{5/2}$, $^4I_{15/2}$→ $^2H_{11/2}$ and $^4I_{15/2}$ → $^4S_{3/2}$ bands, respectively.

on the 4f → 4f transition $^4I_{15/2}$→ $^2H_{11/2}$, and a negative *A*-terms on the $^4I_{15/2}$→ $^4I_{5/2}$ and $^4I_{15/2}$→ $^4S_{3/2}$ transitions. It is well-seen in Fig. 5, that $^4I_{15/2}$→ $^4I_{5/2}$ and $^4I_{15/2}$→ $^4S_{3/2}$ MCD features are of the *C*-type (negative C-terms), since these features have a strong temperature dependence.

In our opinion, the MCD method can be used for the finding of the fluoride nanocrystals doped by the RE-ions in the oxyfluoride glasses, because of the MCD spectrum measured at T = 300K in the oxyfluoride glass ceramic doped with Er^{3+}/Yb^{3+} ions shows a well-resolved structure in contrast to unresolved structure of MCD spectrum measured on an ordinary oxyfluoride glass (see also Fig.4).

MCPL It is well known that the luminescence spectra are suitable for detecting crystal-field levels of the ground and low-energy excited multiplet manifolds of the $4f^n$ and $4f^{n-1}5d$ (or $4f^{n-1}5g$) configurations of the trivalent lanthanide ions [1,2,4,17]. However, in some cases the magnetooptical spectra can help resolve more complicated spectroscopic problems arising at the investigations of the emission spectra. In particular, in this section we explore the possibilities of the magnetic circular polarization of luminescence (MCPL) spectroscopy, which measures the degree of the circular polarization of emission of left- and right-circularly polarized light emitted by the sample magnetized in the longitudinal magnetic field *H* [37, 40].

The major advantage of MCPL over traditional Zeeman luminescence spectroscopy is that MCPL spectra can be recorded in cases where the band width of emission line is larger than its Zeeman splitting. In other words, individual crystal-field levels, which are not resolvable in the luminescence spectra, can be clearly distinguished in the MCPL spectra [37, 40]. At the same time the modeling of MCPL spectra can establish the symmetry and check the reliability of the wave functions of the states connected by magnetooptically active radiative transitions [40].

The spectra of the degree of MCPL recorded in the vicinity of the “red” luminescence band caused by radiative transition $^4I_{9/2}$→ $^4I_{15/2}$ in the oxyfluoride

glass ceramic doped by Er^{3+}/Yb^{3+} ions at T = 90 K, is shown in Fig. 6. Comparison of the spectra of the MCPL degree and luminescence (fluorescence) shows the some structure of the observed magnetooptical spectra $P(\nu)$ on the line - *2* of secondary radiation in oxyfluoride glass ceramic due to radiative transition $^4I_{9/2} \rightarrow {}^4I_{15/2}$ in the Er^{3+} ions. At the same time, a more complex structure of the observed MCPL spectrum in oxyfluoride glass ceramic on the luminescence line - *1* can be

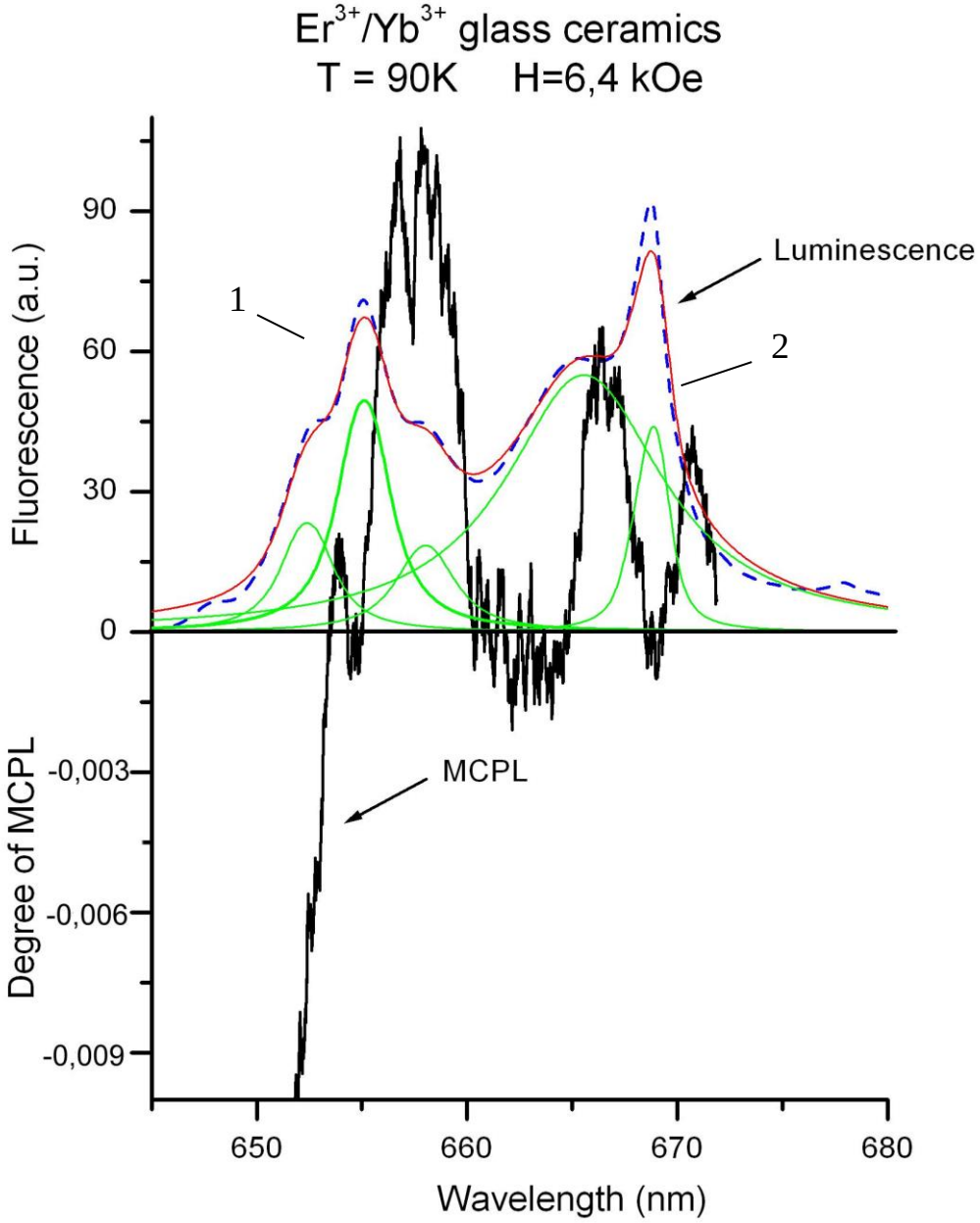

Fig. 6. MCPL spectrum of the oxyfluoride glass ceramic doped by Er^{3+}/Yb^{3+} ions measured at temperature T = 90 K on the 4f → 4f transition $^4I_{9/2} \rightarrow {}^4I_{15/2}$. Decomposition of the luminescence band at 650 - 675 nm observed at T = 90 K is obtained using five Lorentz band profiles.

approximated by the overlapping of the two spectral dependences of linear - type having same values of the slope angle of the *P* dependence is proportional to the "effective" Zeeman splitting $E_{zeem.}$ of the quantum states that are connected by the radiative magnetooptically active 4f → 4f transition and defines value a temperature-independent "diamagnetic" contribution (*A* – term [37,40]) to the MCPL degree on this transition (see also Fig. 6). Note that, the characteristic sharp bend of the MCPL degree feature observed at 655 nm in the oxyfluoride glass ceramic doped by Er^{3+}/Yb^{3+} ions at T = 90 K is clear evidence of the existence of this overlapping (Fig.6).

This dependence is shifted from the line center on the value of the frequency-independent "paramagnetic" pedestal that determines simultaneously the amplitudes of the *C*- and *B*-term of the MCPL degree [37,40]. The contribution of the "paramagnetic" *C*-term of the MCPL degree depends on a difference in sublevel occupations of the initial (or emitting) state of the radiative magnetooptically-active transition, whereas temperature-independent *B*-term corresponds to a contribution to the MCPL degree of so called mechanism of "mixing" by an external magnetic field *H* of the RE- ion quantum states that are connected by the radiative magnetooptically-active 4f → 4f transition [37,40].

Thus, we find that our measurements obtained from the oxyfluoride glass ceramic doped by Er^{3+}/Yb^{3+} ions at T = 90 K shows that on the line - *1* two magnetooptically-active transitions between Stark sublevels of $^4I_{9/2}$ and $^4I_{15/2}$ multiplet manifolds appear simultaneously that may demonstrate an existence of the *quantum cutting effect*. The effect in the visible spectrum appears to be a result of energy transfer (so called "down conversion") in the visible region between neighboring electronic states of Er^{3+} and Yb^{3+} ions in the ceramic glass [41]. The effective energy transfer may be carried out through Er^{3+} excited states assisted by the numerous excited states of Yb^{3+} ions. A similar energy transfer is necessary for the realization of so called "quantum cascade emission" (also called by effect of "*quantum cutting*" [41]), getting more than one photon out for every UV photon absorbed, which is useful at the creation of UV lasers and scintillators.

Therefore, the result of our magnetooptical measurements show, that more interesting method that is useful to establish for the detecting of visible *quantum cutting effect* in the RE-compounds can be method of the magnetic circular polarization of the luminescence (MCPL). The appearance of two quantum transitions in the RE-ions can be accompanied by an essential change of the integral (and other) characteristics of the MCPL line contours.

CONCLUSION

1. We have observed some interesting aspects of the transparent oxyfluoride glass ceramics doped by Er^{3+}/Yb^{3+} ions the magnetooptical and optical properties due to the high optical resolution and sensitivity of the magnetooptical methods providing the reliable detecting of the changes in the energies and linewidths of the optical transitions are caused by an external magnetic field and taking place in the RE-compounds.

2. The absorption spectra in non-polarized light of the oxyflouride glass samples doped by Er^{3+}/Yb^{3+} ions were recorded in the region of the some absorption bands of the Er^{3+} ion at 300 K on a modified single-beam spectrophotometer, which was made on the base of a double diffraction monochromator MDR-23.

3. The MCPL (and luminescence) spectra of the oxyfluoride glass samples doped by Er^{3+}/Yb^{3+} ions were studied in the vicinity of the radiative transition $^4F_{9/2} \rightarrow {}^4I_{15/2}$ (the "red" band of the fluorescence) with spectral resolution ~ 5-10 cm^{-1} near 15400 cm^{-1} in the temperature range 90 - 300 K using a highly sensitive measurement apparatus performed on the base of the double diffraction monochromator MDR-23.

4. To probe the unresolved spectra of the doped by Er^{3+}/Yb^{3+} ions ordinary oxyfluoride glass and oxyfluoride glass ceramic obtained from “Hitachi U- 4100” spectrophotometer, we used a high-resolution double diffraction monochromator MDR Model 23.

5. The MCD method can be used for the finding of the fluoride nanocrystals doped by the RE-ions in the oxyfluoride glasses, because of the MCD spectrum measured at T = 300K in the oxyfluoride glass ceramic doped with Er^{3+}/Yb^{3+} ions shows a well-resolved structure in contrast to unresolved structure of MCD spectrum measured on an ordinary oxyfluoride glass.

REFERENCES

1. G. H. Dieke, *Spectra and Energy Levels of Rare-Earth Ions in Crystals*, Wiley Interscience, New York, 1968.
2. G. H. Dieke, H. M. Crosswhite, and B. Dunn, J. Opt. Soc. Am., **51**, 820 (1961).
3. A. K. Zvezdin, V. M. Matveev, A. A. Mukhin, and A. I. Popov, *Rare Earth Ions in Magnetically Ordered Crystals*, Izdatel Nauka, Moscow, 1985 (in Russian).
4. B. G. Wybourne. *Spectroscopic Properties of Rare Earths*, Interscience, New York, 1965.
5. E. U. Condon and G. H. Shortley, *The Theory of Atomic Spectra*, Cambridge Univ. Press, New York, 1935.
6. L. D. Landau and E. M. Lifshitz, *Quantum Mechanics*, Addison Wesley, Reading, MA, 1958.
7. I. I. Sobelman, *Introduction to the Theory of Atomic Spectra*, Pergamon, New York, 1972.
8. B. R. Judd, *Operator Techniques in Atomic Spectroscopy*, Princeton University Press, 1998 [originally published in 1963].
9. M. V. Eremin, Opt. Spectrosc., **26**, 317 (1969).
10. M. V. Eremin and O. I. Maryakhin, Opt. Spectrosc., **26**, 479 (1969).
11. J.S. Smart, *Effective Field Theories of Magnetism*, Saunders, Philadelphia, 1966.
12. J. H. Van Vleck, *The Theory of Electric and Magnetic Susceptibilities*, Oxford Univ. Press, Oxford, 1932.
13. J. H. Van Vleck, J. Phys. Chem., **41**, 67 (1937).
14. P. A. Tanner, Y. L. Liu, N. M. Edelstein, K. M. Murdoch, N. M. Khaidukov, J. Phys. Cond. Matt., **9**, 7817 (1997).
15. P. A. Tanner. Transition-Metal and Rare-Earth Compounds III: Excited States, Transitions, Interactions, Book Series: *Topics in Current Chemistry*, (Springer, New York, 2004), **Vol. 241**, p. 167.

16. J. Hoshina and S. Kuboniwa, J. Phys. Soc. Jap., **32**,771 (1972).
17. N.V. Starostin, in *Spectroscopy of Crystals*, Izdatel Nauka, Moscow, 1975, p. 12.
18. I.S. Gorban, A.F. Gumenyuk, and V.Ya. Degoda, Opt. Spectrosc., **58,** 278 (1985).
19. W. J. Miniscalco, J. M. Pellegrino, and W. M. Yen, J. Appl. Phys., **49**, 6109 (1978).
20. E. Sarantopoulou, Z. Kollia, A.C. Cefalas, V.V. Semashko, R.Yu. Abdulsabirov, A.K. Naumov, S.L. Korableva, Opt. Commun., **156**, 101 (1998).
21. H. Ebendorff- Heidepriem, D. Ehrt, J. Non-Cryst. Sol., **248**, 247 (1999).
22. U. V. Valiev, A. A. Klochkov, and V. Nekvasil, Opt. Spectrosc., **75**, 33 (1993).
23. L. I. Schiff, *Quantum Mechanics*, McGraw-Hill, New York, 1955.
24. I. S. Edelman, A. V. Malakhovskii, A. M. Potseluyko, T. V. Zarubina, and A. V. Zamkov, J. Non. Cryst. Sol., **306**, 120 (2002).
25. B. R. Judd, Phys. Rev., **127**, 750 (1962).
26. G. S. Ofelt, J. Chem. Phys., **37**, 511 (1962).
27. G. W. Burdick, A. Burdick, V. Deev, C.-K. Duan, and M. F. Reid, J. Lumin., **118**, 205 (2006).
28. S. Washimiya, J. Phys. Soc. Jap., **27**, 56 (1969).
29. E. U. Condon and G. H. Shortley, *The Theory of Atomic Spectra*, Cambridg Univ. Press, New York, 1935.
30. G. Racah, Phys. Rev., **63**, 367 (1943).
31. C. Görller-Walrand and K. Binnemans, in *Handbook on the Physics and Chemistry of Rare Earths*, edited by K. A. Gschneidner, Jr. and L. Eyring, North-Holland, Amsterdam, 1998, Vol. 25, p. 101.
32. J. D. Axe, J. Chem. Phys., **39**, 1154 (1963).
33. M. J. Weber, Phys. Rev., **171**, 283 (1968).

34. W. T. Carnall, G. L. Goodman, K. Rajnak, and R. S. Rana, J. Chem. Phys., **90**, 3443 (1989)

35. K. Binnemans, D. Verboven, C. Gorller-Walrand, J. Lucas, N. Duhamel-Henry, J.L. Adam, J. of Alloys and Comp. **250**, 321 (1997).

36. LUO Shi Qiang, ZHAO Li Juan, HU Nan, ZHANG Ming, ZHANG Pan, WANG Ya-Zhou, YU Hua, Chin. Phys. Lett., Vol. **2**8, No. 3, 034207 (2011)

37. U.V. Valiev, J.B. Gruber, B. Zandi, U.R. Rustamov, A.S. Rakhmatov, D.R. Dzhuraev, and N.M. Narzullaev, Phys. Stat. Sol. (b) **242**, 933 (2005).

38. Badoz J., Billardon M., Canit J.C., Russel J. Sensitive devices to deterimine the state and degree of polarization of a light beam using a birefringence modulation // J.Opt. (Paris), **8**, No6, 373-384, (1977)

39. U.V. Valiev, T. Asilov, and R.A. Salykov, Instrum. Exper. Techn. **4**, 449 (1994).

40. U.V. Valiev, J.B. Gruber, G.W. Burdick, *Magnetooptical Spectroscopy of the Rare - Earth Compounds: Development and Application* (Scientific Research Publishing, USA, 2012) p.139.

41. K.D. Oskam, R.T. Wegh, H. Donker, E.V.D. van Loef, A. Meijerink, J. of Alloys and Comp., **300-301,** 421 (2000).